iScience

CellPress
OPEN ACCESS

Article

Moraxella catarrhalis evades neutrophil oxidative stress responses providing a safer niche for nontypeable *Haemophilus influenzae*

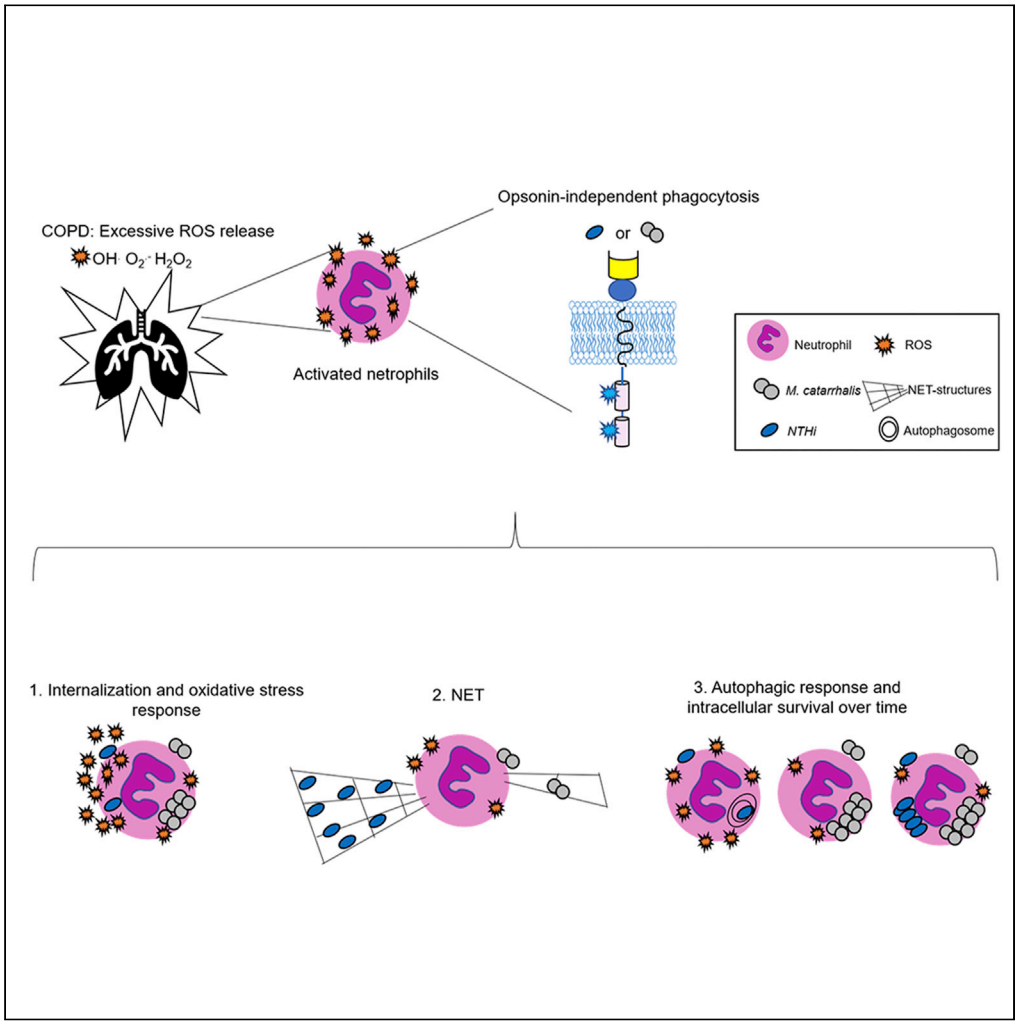

Sonia Nicchi, Fabiola Giusti, Stefano Carello, ..., Vincenzo Scarlato, Domenico Maione, Cecilia Brettoni

domenico.x.maione@gsk.com (D.M.)
cecilia.x.brettoni@gsk.com (C.B.)

Highlights

Mcat induces ROS and NET production to a lesser extent than NTHi in dHL-60 cells

Mcat interferes with ROS-related responses in chemically-activated cells

Mcat subverts the autophagic pathway surviving intracellularly while NTHi does not

Intracellular survival of NTHi is enhanced by the co-infecting bacterium Mcat

Nicchi et al., iScience *25*, 103931
March 18, 2022
https://doi.org/10.1016/j.isci.2022.103931

iScience

CellPress
OPEN ACCESS

Article

Moraxella catarrhalis evades neutrophil oxidative stress responses providing a safer niche for nontypeable *Haemophilus influenzae*

Sonia Nicchi,[1,2] Fabiola Giusti,[1] Stefano Carello,[1,3] Sabrina Utrio Lanfaloni,[1] Simona Tavarini,[1] Elisabetta Frigimelica,[1] Ilaria Ferlenghi,[1] Silvia Rossi Paccani,[1] Marcello Merola,[1,4] Isabel Delany,[1] Vincenzo Scarlato,[2] Domenico Maione,[1,*] and Cecilia Brettoni[1,5,*]

SUMMARY

***Moraxella catarrhalis* and nontypeable *Haemophilus influenzae* (NTHi) are pathogenic bacteria frequently associated with exacerbation of chronic obstructive pulmonary disease (COPD), whose hallmark is inflammatory oxidative stress. Neutrophils produce reactive oxygen species (ROS) which can boost antimicrobial response by promoting neutrophil extracellular traps (NET) and autophagy. Here, we showed that *M. catarrhalis* induces less ROS and NET production in differentiated HL-60 cells compared to NTHi. It is also able to actively interfere with these responses in chemically activated cells in a phagocytosis and opsonin-independent and contact-dependent manner, possibly by engaging host immunosuppressive receptors. *M. catarrhalis* subverts the autophagic pathway of the phagocytic cells and survives intracellularly. It also promotes the survival of NTHi which is otherwise susceptible to the host antimicrobial arsenal. In-depth understanding of the immune evasion strategies exploited by these two human pathogens could suggest medical interventions to tackle COPD and potentially other diseases in which they co-exist.**

INTRODUCTION

Chronic obstructive pulmonary disease (COPD) is a chronic multifactorial inflammatory disease whose main pathophysiological mechanisms include airflow limitation, pulmonary emphysema, and chronic bronchitis (Decramer et al., 2012; Brown, 2018). The course of COPD is marked by recurrent periods of worsening symptoms, called exacerbations (Pavord et al., 2016), responsible for disease progression, increased morbidity and mortality. Several epidemiological studies have reported that nontypeable *Haemophilus influenzae* (NTHi) and *M. catarrhalis* are the most prevalent bacteria found in the sputum of individuals with exacerbations of COPD (Naito et al., 2017; Pavord et al., 2016, D'anna et al., 2020) and their co-infections reach up to 20–30% (Perez and Murphy, 2019).

Among the aspects that characterize COPD pathogenesis, neutrophil-mediated oxidative stress (or reactive oxygen species, ROS) is one of the most important hallmarks (Choudhury and Macnee, 2017;Jaroenpool et al., 2016). There is significant theoretical support for the hypothesis that ROS contributes to the pathogenesis of COPD (Footitt et al., 2016). Lungs *per se* are particularly vulnerable to oxidative stress due to the relatively high oxygen environment, increased blood supply, and exposure to environmental pathogens and toxins. Additional factors contributing significantly to this burden are cigarette smoke and, in COPD patients under treatment, extensive antibiotic exposure (Marino et al., 2015). In severe COPD, ROS generation is markedly enhanced due to the presence of activated neutrophils which also represent the predominant inflammatory cell types (Di Stefano et al., 2004). In response to the presence of microbes and/or the activation of pattern recognition receptors (PRRs), neutrophils produce ROS as a powerful antimicrobial weapon to curtail bacterial infections (Nguyen et al., 2017). ROS production is accomplished by the multicomponent NADPH oxidase complex (NOX2) and complex I, II, and III within the mitochondrial respiratory chain (Glasauer and Chandel, 2013; Dan Dunn et al., 2015; El-Benna et al., 2009). ROS are released both extracellularly at the site of infection and intracellularly following bacterial phagocytosis (Dupre-Crochet et al., 2013). Most pathogens survive the action of ROS by employing intrinsic

[1]GSK, Siena, 53100, Italy

[2]University of Bologna, Bologna, 40141, Italy

[3]University of Turin, Turin, 10100, Italy

[4]University of Naples Federico II, Naples, 80133, Italy

[5]Lead contact

*Correspondence: domenico.x.maione@gsk.com (D.M.), cecilia.x.brettoni@gsk.com (C.B.)

https://doi.org/10.1016/j.isci.2022.103931

mechanisms such as detoxification of radical species, metal homeostasis, and DNA damage repair systems (Imlay, 2008). Additionally, a few bacterial pathogens exploit extrinsic resistance mechanisms to actively suppress ROS production by eukaryotic cells, as in the case of *Pseudomonas aeruginosa* or *Chlamydia trachomatis* through a contact-dependent mechanism and the expression of extracellular effector, respectively (Vareechon et al., 2017; Rajeeve et al., 2018). Others bacteria, such as *Franciscella tularensis* and *Neisseria gonorrhoeae* not expressing opa proteins, essentially disrupt NADH oxidase activity by not fully elucidated mechanisms (Mccaffrey et al., 2010; Smirnov et al., 2014). Some bacteria take advantage of the oxidative environment eliciting the respiratory burst. For example, in *Haemophilus pylori* pathogenesis, ROS production leads to an increased eukaryotic lipid peroxidation and membrane damages exacerbating peptic ulcer disease (Perez et al., 2017).

ROS release boosts the overall microbicidal activities and is thought to stimulate neutrophil extracellular traps (NETs) (Nguyen et al., 2017; Zeng et al., 2019) and autophagy (Deretic et al., 2013). NETs are web-like extracellular structures that are the result of decondensed chromatin associated with histones and enzymes such as neutrophil elastase (NE) and myeloperoxidase (MPO) (Aratani, 2018). NETs enable the capture of pathogens within bactericidal DNA-protein aggregates, thereby limiting their spread (Delgado-Rizo et al., 2017). Although the term autophagy means 'to digest oneself', it is now clear that autophagy is also involved in the eradication of intracellular pathogens ("xenophagy") (Jo et al., 2013). The formation of the double-membrane autophagosomes requires two ubiquitin-like conjugation systems, one of which is the microtubule-associated protein light chain 3 (LC3). LC3 is lipidated during the activation of autophagy generating the LC3-II (LC3-B) form which associates with autophagosomes (Deretic et al., 2013). These defense mechanisms, ROS, NET and xenophagy, represent key inflammatory responses in COPD (Porto and Stein, 2016).

Considering the increasing clinical relevance of *M. catarrhalis* and NTHi in COPD, we decided to shed light on the mechanisms underlying the interactions between these bacteria and neutrophils, focusing on the pathways related to the oxidative stress response. It has been reported that interactions between *M. catarrhalis* UspA1 autotransporter and NTHi P5 proteins with carcinoembryonic antigen-related cellular adhesion molecule CEACAM-3 receptor on granulocytes are responsible for neutrophil-mediated phagocytosis (Schmitter et al., 2004). CEACAM-3, which is exclusively expressed in neutrophils (Bonsignore et al., 2019), triggers not only opsonin-independent bacterial phagocytosis but also oxidative burst and degranulation responses (Buntru et al., 2011). It has also been reported that the interaction of *M. catarrhalis* UspA1 with CEACAM-3 is important for its ability to elicit oxidative bursts and degranulation responses in nonstimulated human granulocytes (Heinrich et al., 2016). NTHi has been shown to induce high oxidative stress and NETs formation both in the lungs of BALB/c mice (King et al., 2015) and in a tissue culture model (Kalograiaki et al., 2016). In our study, we used exponentially-growing *M. catarrhalis* BBH18 strains (De Vries et al., 2010) and NTHi 658 strains (Mayhew et al., 2018), clinical isolates derived from COPD patients during the exacerbation state, to challenge human HL-60 cell line, differentiated into neutrophil-like cells (dHL-60) or primary cells. We demonstrated that, differently from NTHi, *M. catarrhalis* is able to dampen the host innate immune response by directly interfering with ROS production and ROS-related responses in a phagocytosis and opsonins-independent but contact-dependent manner. Furthermore, under co-infection experiments, NTHi intracellular survival is enhanced by the co-infecting bacterium *M. catarrhalis* which therefore provides a safer niche for NTHi.

RESULTS

M. catarrhalis and NTHi: Two different ways to interact with neutrophil-like cells

We first investigated the interaction and opsonin-independent uptake of *M. catarrhalis* and NTHi with differentiated neutrophil-like cells (dHL-60). HL-60 cells represent the most commonly used cell line to study different neutrophilic immunological responses since certain signaling pathways, such as protein kinase C (PKC) activation, are difficult to detect in primary neutrophils (Rajeeve et al., 2018). The dHL-60 cells were chemically activated *in vitro* by treatment with Phorbol 12-Myristate 13-Acetate (PMA) to induce strong activation of the oxidative burst. We challenged activated dHL-60 cells with or without cytochalasin D, a known inhibitor of phagocytosis, with exponentially growing, nonopsonized *M. catarrhalis* or NTHi (MOI, MOI = 50) for 20-, 45- and 75 min at 37°C. After incubation, samples were fixed, permeabilized, and then *M. catarrhalis* or NTHi were stained with bacteria-specific polyclonal anti-sera. dHL-60 cells were analyzed by flow cytometry to measure the percentage of cells associated to bacteria (untreated samples) or the percentage of cells with bacteria attached and not internalized (cytochalasin D-treated

samples). Results are reported in Figure 1, panels A and B. The percentage of phagocytosis (light blue bars) was calculated by subtracting the percentage of adhesion (green bars) from the total interaction and the consequent percentage of non-infected cells was reported (red bars). As can be observed in Figure 1A, *M. catarrhalis* was rapidly internalized into neutrophil-like cells as the percentage of cells showing internalized bacteria was 18.4% already 20 min post-infection. The total association of *M. catarrhalis* to activated dHL-60 cells increased over time (host cells with internalized bacteria passed from 18.4% to 43.25%) with the percentage of non-infected cells ranging from 38.3% to 17.5% at 20- and 75 min, respectively, otherwise only 3.3% of cells with internalized NTHi bacterial cells was recorded at 20 min post-infection (Figure 1B), and a completely different kinetic of internalization compared to that of *M. catarrhalis* was observed. The percentage of cells with phagocytosed bacteria slightly increased to 15.2% at 75 min with the percentage of non-infected cells ranging from 90% to 73.3% at 20- and 75 min, respectively.

To visualize these adhesion and invasion phenomena, transmission electron microscopy was performed on PMA-activated dHL60 cells whether infected or not (control) by non-opsonized *M. catarrhalis* or NTHi at MOI of 50 for 20- and 75 min. Representative images of electron microscopy cross sections are reported in Figure 1C. At 20 min post-infection, *M. catarrhalis* bacteria formed grape-like aggregates on the cell surface, the host cell exhibited membrane protrusion or lamellipodia at the site of contact with bacteria. Of interest, at 20 min post-infection, bacteria were found in early stages of phagocytosis but also in phagolysosomes (bacteria surrounded by electrodense materials). When dHL-60 cells were infected by NTHi, a small portion of the host cells were found to be infected and a few bacterial cells were visibly phagocytosed at 20 min post-infection. At 75 min, neutrophil-like cells were packed with a high number of *M. catarrhalis* and intact mitochondria and heterochromatin condensation of nuclei were detected. Differently from *M. catarrhalis*, at 75 min post-infection with NTHi, events of apoptosis such as extensive cytoplasmic vacuolizations were detected despite only a low amount of bacteria being phagocytosed. These observations suggest that while a small number of NTHi bacterial cells remains intracellularly, *M. catarrhalis* is rapidly internalized into neutrophil-like cells in an opsonin-independent manner and accumulated over time blocking any cell response to clear the pathogen.

M. catarrhalis actively interferes with cellular ROS production while NTHi does not

We subsequently investigated the potential impact of *M. catarrhalis* and NTHi on the respiratory burst, a key weapon of innate immunity against invading microorganisms. To this purpose, we challenged dHL-60 cells with non-opsonized *M. catarrhalis* or NTHi (MOI = 50) and measured the intracellular ROS production by flow cytometry at 60-, 120- and 240-, min post-infection using CellROX fluorogenic dye. Measurements of the mean fluorescence intensities (MFI) from infected cells, normalized by fluorescence signals of uninfected cells, are reported in Figure 2A. Results showed that *M. catarrhalis* barely induced an oxidative stress response in dHL-60 cells (MFI of 404 and 1692 at 60 and 240 min, respectively) while NTHi showed a marked increase of oxidative burst over time (MFI of 796 and 14,994 at 60 and 240 min, respectively). In fact, the recorded MFIs obtained in cells infected by NTHi were significantly higher compared to that measured for *M. catarrhalis* at 120 and 240 min post-infection.

Next, we asked if *M. catarrhalis* and NTHi were able to actively interfere with ROS production in chemically activated dHL-60 cells by using the aforementioned dye, CellROX. We treated uninfected cells (red lines) or cells infected with bacteria at MOI of 50 (blue lines) with PMA (Figure 2C) and the resulting MFIs were evaluated at 30, 60, 90 and 120 min post-infection by flow cytometry. As shown in Figure 2B, intracellular ROS production in PMA-stimulated cells was dampened by *M. catarrhalis* infection and this effect was not due to cell death (Figure S1). By contrast, no reduction in ROS generation was observed when cells were infected by NTHi at any of the indicated time points (Figure 2C). Subsequently, we verified if Mcat suppression was also effective on the extracellular ROS production. dHL-60 cells were left uninfected or infected with bacteria at different ratios (MOI of 100, 50, 25 and 12) and treated with PMA. The kinetics of the oxidative burst response was measured every 3 min within 2 h by using a luminol-dependent chemiluminescence assay. As can be observed in Figure 2D, the exposure to PMA of uninfected dHL-60 cells showed a peak of luminescence at 42 min of treatment. When stimulated cells were infected by *M. catarrhalis*, the extracellular ROS production was suppressed in a MOI-dependent manner

From the above data we conclude that unlike NTHi, *M. catarrhalis* does not induce a strong oxidative response in non-stimulated cells and is able to dampen ROS generation in chemically activated neutrophil-like cells.

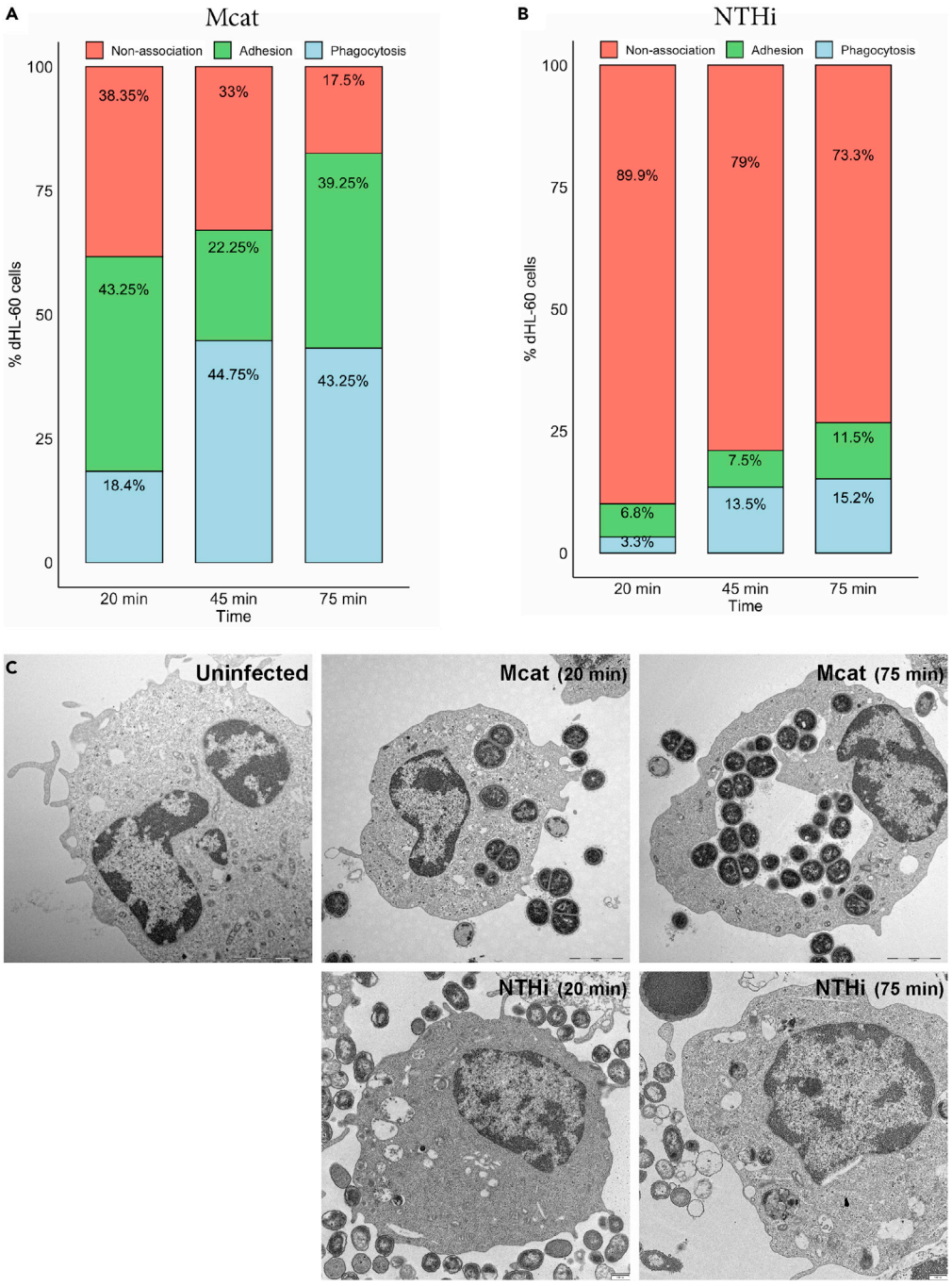

Figure 1. *M. catarrhalis* and NTHi: two different ways to inteact with neutrophil-like cells

(A and B) PMA-stimulated dHL-60 cells were treated with cytochalasin D (for bacterial adhesion) or untreated (total association). They were infected with *M. catarrhalis* (A) or NTHi.

(B) at MOI 50 for 20-, 45- and 75 min. Cells were fixed, permeabilized and bacteria were detected by staining for UspA2 (rabbit polyclonal antibodies) or for whole bacteria for *M. catarrhalis* (A) or NTHi (B), respectively. dHL-60 cells were evaluated by flow cytometry and expressed as the percentage of bacteria positive-cells. Red bars: noninfected cells; Green bars: adhesion; and light blue bars: phagocytosis.

(C) Transmission electron microscopy for uninfected PMA-activated dHL60 cells (left panel) and infected by non-opsonised *M. catarrhalis* (top panels) or NTHi (bottom panels) at MOI 50 for 20 min and 75 min. Scale bars, 2 μm.

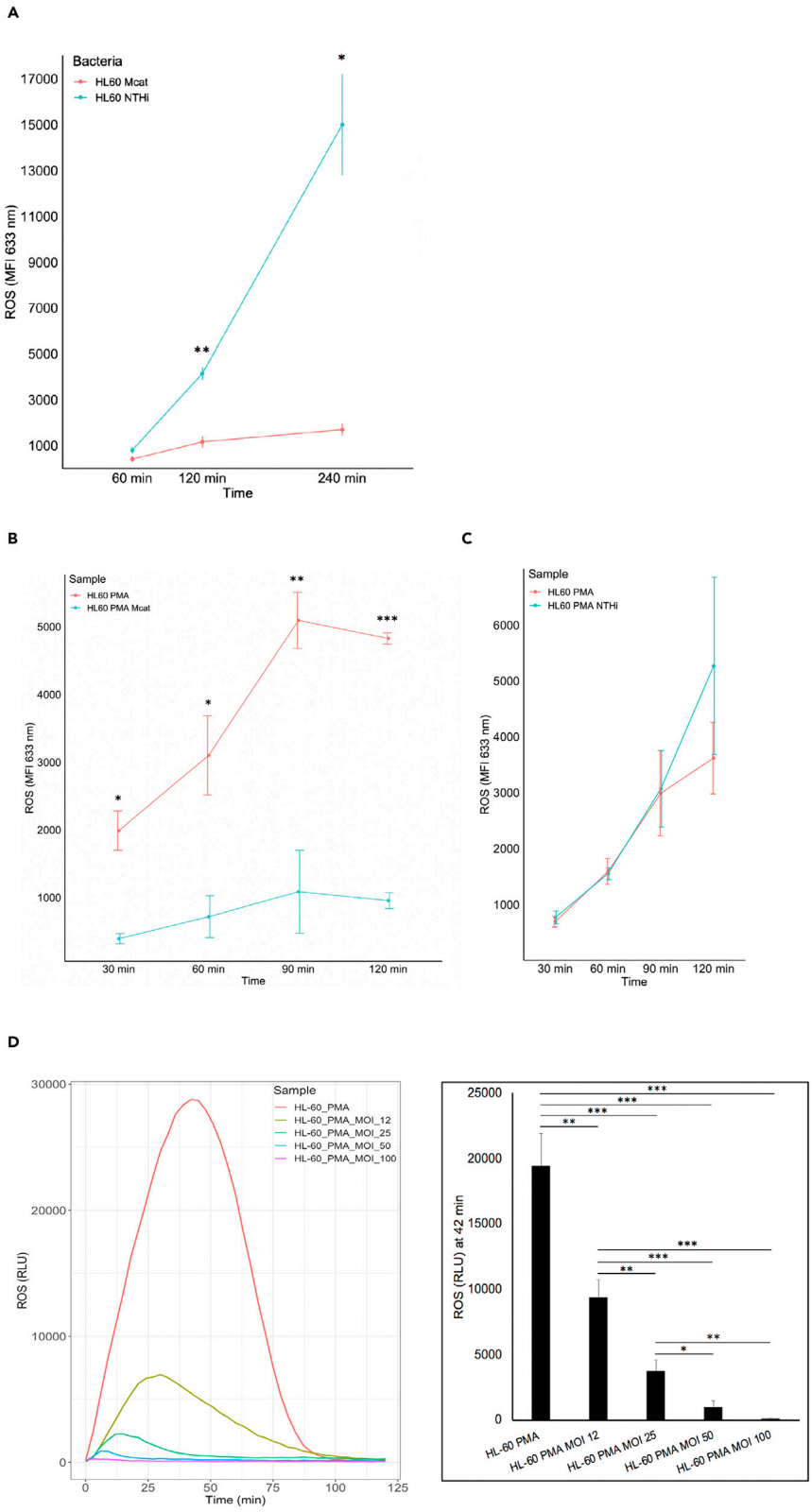
A
Bacteria
HL60 Mcat
HL60 NTHi
ROS (MFI 633 nm)
Time
60 min
120 min
240 min
B
Sample
HL60 PMA
HL60 PMA Mcat
ROS (MFI 633 nm)
Time
30 min
60 min
90 min
120 min
C
Sample
HL60 PMA
HL60 PMA NTHi
ROS (MFI 633 nm)
Time
D
Sample
HL-60_PMA
HL-60_PMA_MOI_12
HL-60_PMA_MOI_25
HL-60_PMA_MOI_50
HL-60_PMA_MOI_100
ROS (RLU)
Time (min)
ROS (RLU) at 42 min
HL-60 PMA
HL-60 PMA MOI 12
HL-60 PMA MOI 25
HL-60 PMA MOI 50
HL-60 PMA MOI 100

Figure 2. *M. catarrhalis* actively interferes with cellular ROS production while NTHi does not

Differentiated HL-60 cells were infected with the *M. catarrhalis* BBH18 or NTHi 658 at the indicated MOI and ROS production was monitored over time using a fluorogenic dye CellROX (intracellular ROS) and chemiluminescence (extracellular ROS).

(A) Differentiated HL-60 cells were infected with the *M. catarrhalis* BBH18 or NTHi 658 at MOI 50 and ROS production at 1, 2 and 4h post-infection was monitored using a fluorogenic dye, CellROX (intracellular ROS). MFI at 633 nm from at least three independent experiments at the indicated time point after infection was determined by flow cytometry and was the result of subtraction from fluorescence signals of uninfected cells for the corresponding time point. Bars represent means ± SE. MFI, Mean fluorescence intensity. *$p < 0.05$; **$p < 0.01$; ***$p < 0.001$.

(B and C) dHL60 cells were stimulated for ROS production and infected with *M. catarrhalis* BBH18 (B) or NTHi 658 (C) at MOI 50. MFI at 633 nm from at least three independent experiments at the indicated time point after infection was determined by flow cytometry. Bars represent means ± SE. MFI, Mean fluorescence intensity. *$p < 0.05$; **$p < 0.01$; ***$p < 0.001$.

(D) dHL60 cells were stimulated for ROS production and infected with *M. catarrhalis* BBH18 at MOI 100, 50, 25 and 12. Representative experiment showing generation of chemiluminescence measured every 3 min within 2 h along with the quantification of ROS at 42 min from at least three independent experiments. Bars represent means ±SE RLU, relative luminescence units. *$p < 0.05$; **$p < 0.01$; ***$p < 0.001$ by chemiluminescence

M. catarrhalis limits ROS production in a contact-dependent and phagocytosis-independent manner by possibly binding immunosuppressive receptors

To better characterize the mechanisms by which *M. catarrhalis* actively interferes with ROS production in host cells, we examined whether the suppression was mediated by bacterial secreted products or by direct bacterial contact with dHL-60 cells. To this aim, we measured internal and external ROS production on dHL-60 cells treated with conditioned supernatants of infected cells (Figures 3A and S2A) or cytochalasin D, known to inhibit phagocytosis (Figures 3B and S2B). dHL-60 cells were infected by *M. catarrhalis* (MOI 50) and at 42 min post-infection (the time point at which the peak of ROS production in PMA-stimulated cells was recorded), the resulting supernatant was collected and exposed to naive cells. Under these conditions, no suppression of the PMA-induced oxidative response was observed (Figures 3Aand S2A), suggesting that the observed mechanism was likely to be mediated by factors not released in supernatants derived from *M. catarrhalis* infecting dHL-60 cells. By performing an experiment with bacterial supernatant only, we showed that suppression of ROS was not related to Mcat secreted products after growth in BHI medium (Figure S2C). Subsequently, we examined whether the bacterium requires internalization by the host cells to exert its inhibitory effect. In this regard, untreated or cytochalasin D-treated dHL-60 were left uninfected or challenged with Mcat. In the presence or absence of this molecule, the extent of ROS inhibition in PMA-stimulated infected dHL-60 cells remained largely unchanged (Figures 3B and S2B), indicating that the bacterial internalization in dHL-60 cells was not necessary to suppress ROS production. These results suggest that *M. catarrhalis* impairs the oxidative stress response in chemically activated cells with a mechanism that is contact-dependent, phagocytosis-independent and not related to the secretion of effector proteins or toxins.

It is known that neutrophil activation and subsequent ROS response is controlled by a number of cell surface receptors including both immunoactivating and also immunosuppressive receptors (Futosi et al., 2013). As we have ascertained that a bacteria-cell contact mechanism is necessary for down-regulation of the oxidative stress response, the ability of Mcat to bind to immunosuppressive receptors has been investigated. Several inhibitory receptors such as some Siglec receptors (Siglec-5 and Siglec-9) and receptors of the CEACAM family (such as CEACAM-1) regulate the immune response mainly by blocking activating pathways (Pyz et al., 2006). To this purpose, *M. catarrhalis* was incubated or not, with 2 μg of each recombinant protein: CEACAM-1 (known interactor of the Mcat UspA1 protein) (Brooks et al., 2008), Siglec-5 and Siglec-9 inhibitory receptors. Binding of these soluble proteins to the bacteria was revealed by flow cytometry using antibodies specific to each recombinant receptor. As shown in Figure 3C, the MFI obtained after incubation of the soluble recombinant proteins CEACAM-1, Siglec-5 and Siglec-9 were statistically different from their controls (bacterial cells incubated with the corresponding antibody without the protein of interest). These data suggest that in addition to CEACAM-1 binding, *M. catarrhalis* is able to bind also the immunosuppressive Siglecs receptors (Siglec-5 and Siglec-9). To verify if these human receptors are indeed those specifically bound by Mcat to dampen ROS production, we challenged PMA-activated dHL-60 cells with *M. catarrhalis,* untreated or pre-incubated with 200 nM of each recombinant receptor. The intracellular ROS production was evaluated by flow cytometry at 120 min post-infection using CellROX dye. As shown in Figure 3D, when Mcat was incubated with CEACAM1 or Siglec-5, the observed interference with intracellular ROS production by PMA-activated infected cells was

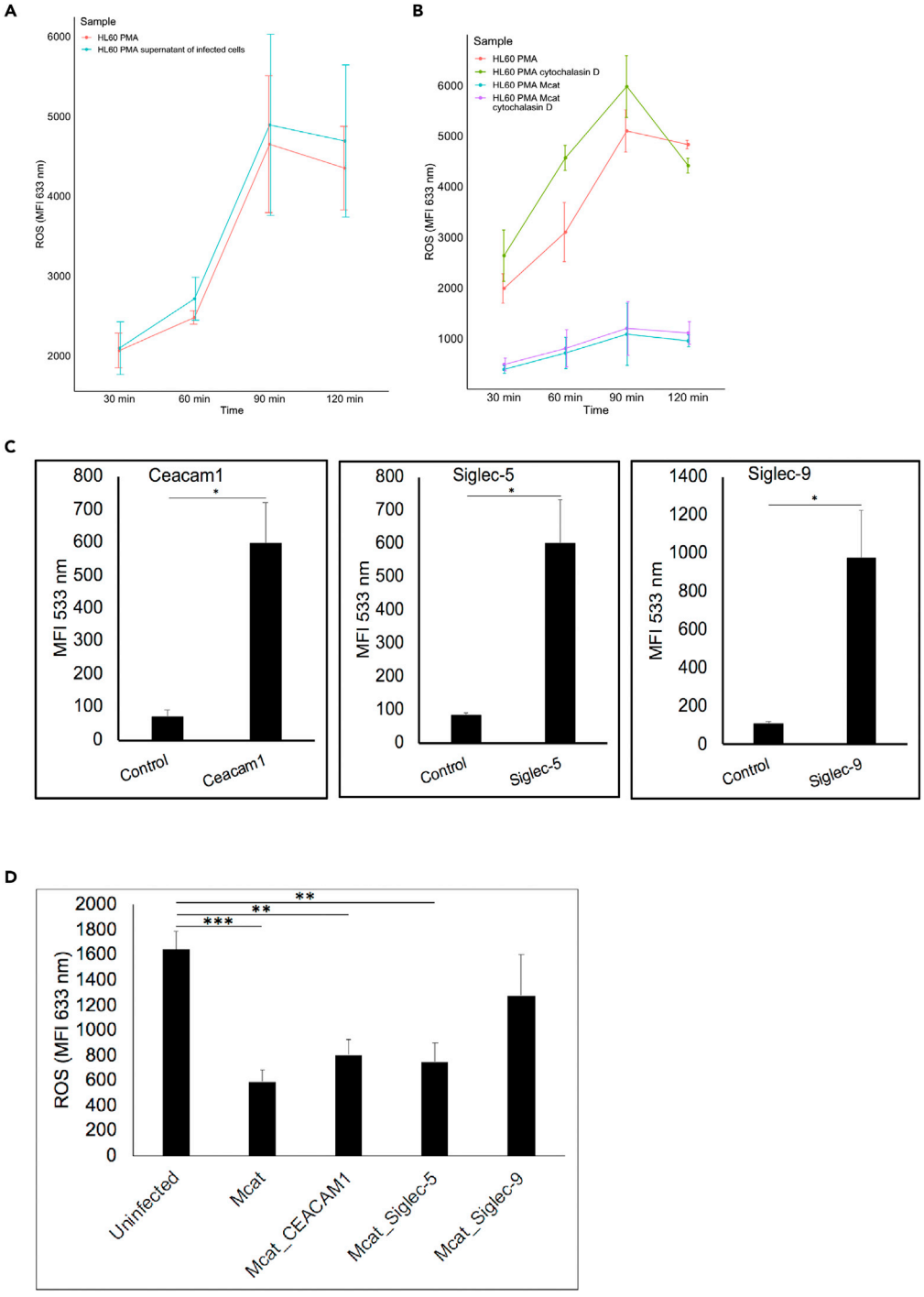

Figure 3. *M. catarrhalis* limits ROS production in a contact-dependent and phagocytosis-independent manner by possibly binding immunosuppressive receptors

(A) dHL-60 were infected or not by *M. catarrhalis* BBH18 strain (MOI 50) and the resulting supernatants were presented to naive ROS-induced cells.

(B) ROS-induced dHL60 cells were pre-incubated with cytochalasin D (phagocytosis inhibitor) and infected with *M. catarrhalis* BBH18 at MOI 50. (A and B) MFI at 633 nm from at least three independent experiments at the indicated time point after infection was determined by flow cytometry. Bars represent means ± SE. MFI, Mean fluorescence intensity.

Figure 3. *Continued*

(C) *M. catarrhalis* was incubated or not (control) with 2 μg of each human recombinant protein: CEACAM-1, Siglec-5 and Siglec-9. Antibodies raised against the recombinant proteins were used for detection by flow cytometry. MFI at 535 nm from at least three independent experiments. Bars represent means ± SE. MFI, Mean fluorescence intensity. *$p < 0.05$.
(D) *M. catarrhalis* was pre-incubated or not (control) with 200 nM of each human recombinant protein: CEACAM1, Siglec-5 and Siglec-9. dHL60 cells were stimulated for ROS production and infected with Mcat (control), Mcat_CEACAM1, Mcat_Siglec-5 or Mcat_Siglec-9 at MOI of 50. MFI at 633 nm from at least three independent experiments at 2 h post-infection was determined by flow cytometry. Bars represent means ± SE. MFI, Mean fluorescence intensity. **$p < 0.01$; ***$p < 0.001$.

only slightly affected. Interestingly, the recorded MFI obtained after the incubation with the recombinant Siglec-9 receptor was similar to that recorded for the uninfected PMA-activated cells. These data suggest that blocking the cognate binding Siglec-9 partner prevents the specific binding between bacteria and dHL60 cells and as a result Mcat is no longer able to interfere with ROS.

NET generation is differently modulated by NTHi and *M. catarrhalis*

As NETs are major contributors to chronic inflammatory and lung tissue damage in COPD (Grabcanovic-Musija et al., 2015), we investigated NET formation in cells infected with *M. catarrhalis* or NTHi individually and in combination. For this purpose, dHL-60 cells were infected with *M. catarrhalis* or NTHi at MOI 50, or with both bacteria (MOI 25 each) for 4 h. The cells treated with PMA (positive control for NET formation) were subsequently infected or not with *M. catarrhalis* (MOI 50). We quantified the extracellular DNA associated with NET formation and visualized these structures by confocal and electron microscopy. For the quantification, the supernatants of these samples were removed to exclude free/degraded NETs-DNA and necrotic DNA. Samples were then treated with micrococcal nuclease and the amount of extracellular DNA in the resulting supernatants was quantified using PicoGreen staining. No significant differences in NET-associated DNA of non-stimulated cells or infected by *M. catarrhalis* (MOI 50) were measured (18.7 and 24.7 ng/ml, respectively) while infection of dHL-60 cells with NTHi (MOI 50) or treatment with PMA (positive control) resulted in high amounts of NET-associated DNA (66.3 and 107.1 ng/ml, respectively) (Figure 4A). Non-stimulated cells, when co-infected by *M. catarrhalis* and NTHi released an intermediate amount of NET-associated DNA (40.3 ng/ml) with respect to individual infections with *M. catarrhalis* or NTHi. Interestingly, NET-associated DNA of PMA-activated dHL-60 cells infected by *M. catarrhalis* was nearly three times lower than that of the positive control (35.9 ng/ml and 107.1 ng/ml, respectively) (Figure 4A). The same observations can be made from the images obtained by scanning electron microscopy (Figures 4B and S3) and confocal microscopy (DNA and myeloperoxidase, MPO, are visualized in blue and green, respectively) (Figure 4C), where networks of DNA and MPO extracellular fibers were clearly visible in dHL-60 cells treated with PMA. NTHi was surrounded by these web-like extracellular microbicidal structures and partially rescued when *M. catarrhalis* was present. From the above data, we conclude that *M. catarrhalis* does not cause significant NET release in infected cells while NTHi, as expected, induces more NETosis. Moreover, *M. catarrhalis* is able to suppress NET generation in PMA-stimulated cells or dHL-60 cells infected by NTHi.

M. catarrhalis interferes with the autophagic pathway surviving intracellularly and reducing the killing of NTHi

Next, we focused on the impact of *M. catarrhalis* on the autophagic pathway. To characterize this response, PMA-activated dHL-60 cells were left uninfected or incubated with *M. catarrhalis* or NTHi at MOI 50 for 40 min. The non-adherent bacteria were washed away and gentamicin was added for 20 min to inhibit growth of extracellular bacteria. From this time on (1 h, control group), samples were incubated for an additional 3 h in the presence of PMA (Figure 5A). At these two time points (1h and 4h), samples were fixed and the autophagic response was monitored by flow cytometry, staining the cells for LC3-II marker. As can be observed from the MFI in Figure 5B, the expression of LC3-II is 2.5-fold lower in cells infected by *M. catarrhalis* compared to the uninfected ones. By contrast, uninfected cells and cells infected by NTHi showed similar LC3-II expression levels (Figure 5B). These data indicate that while NTHi infected cells shows an autophagic response, *M. catarrhalis* is able to interfere with the autophagic response in dHL-60 cells.

Transmission Electron Microscopy (TEM) analysis was performed at different time points of the assay shown in Figure 5A and representative images of electron microscopy cross sections are reported in Figure 5C. As can be observed, after 1 h, uninfected cells displayed an intact membrane and progressive margination

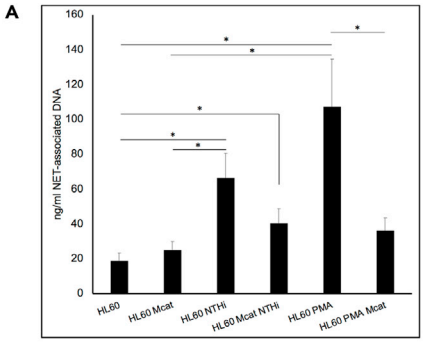
A
ng/ml NET-associated DNA
160
140
120
100
80
60
40
20
0
HL60
HL60 Mcat
HL60 NTHi
HL60 Mcat NTHi
HL60 PMA
HL60 PMA Mcat

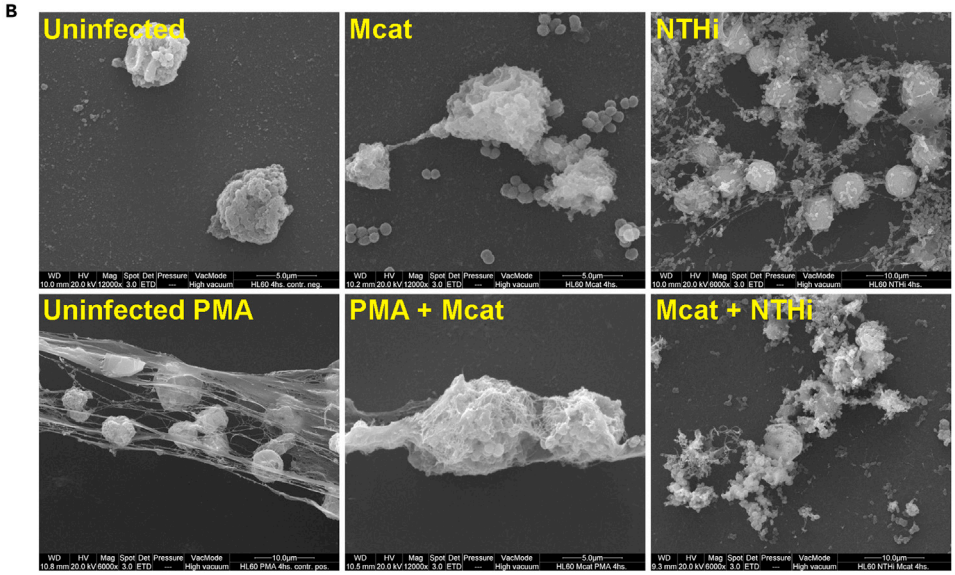
B
Uninfected
Mcat
NTHi
Uninfected PMA
PMA + Mcat
Mcat + NTHi

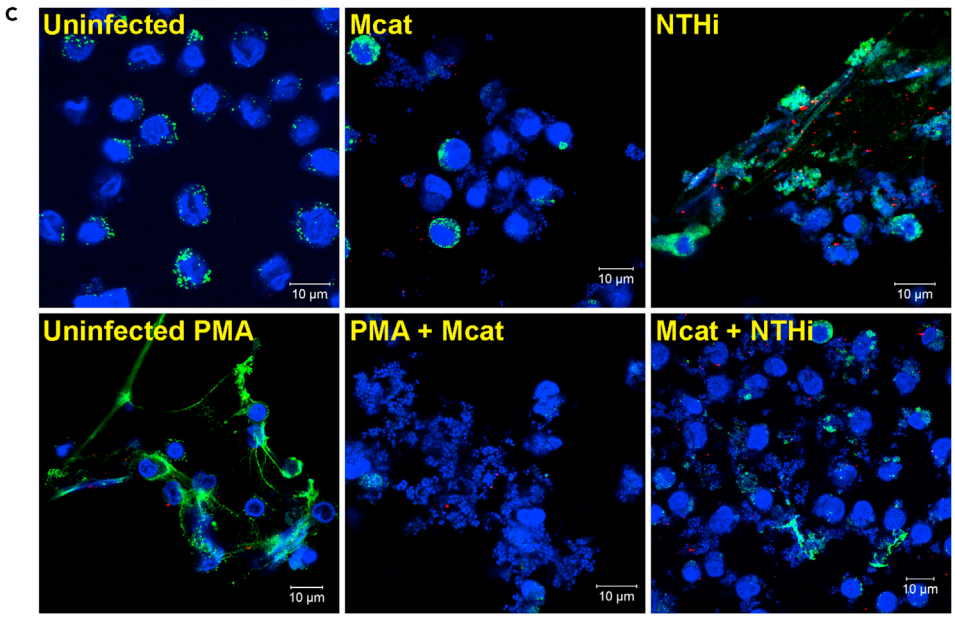
C
Uninfected
Mcat
NTHi
Uninfected PMA
PMA + Mcat
Mcat + NTHi
10 µm

Figure 4. NET generation is differently modulated by NTHi and *M. catarrhalis* dHL-60 cells were left untreated, or either infected singly with *M. catarrhalis*

(MOI 50) or NTHi (MOI 50), or with a combination of the two bacteria (MOI 25 each). dHL-60 were also treated with a known inducer of NETs (PMA) and infected or not with *M. catarrhalis* (MOI 50). The reaction was allowed to proceed for 4h.
(A) Samples were centrifuged, nuclease-treated and the amount of DNA in the supernatant was quantified using PicoGreen (Invitrogen) staining and the fluorescence was detected at 530 nm using a TECAN Infinite 200 plate reader. Λ DNA at known concentrations was used as standard. Each sample was processed in triplicate to avoid any bias in the reading. From a standard curve obtained by using known concentration of λ DNA, the ng/ml of NET-associated DNA was determined. The resulting graph is obtained from seven independent experiments. Bars represent means ±SE *$p < 0.05$.
(B) Samples were fixed and analyzed by scanning electron microscopy. Scale bars, 5- or 10 μm.
(C) dHL-60 cells were fixed with 4% paraformaldehyde and stained for DNA (DAPI, blue) or myeloperoxidase (MPO, green) The stained cells were analyzed by immunofluorescence microscopy. Scale bars, 10 μm.

and compacting of chromatin beneath the nuclear envelope witnessing the presence of early stages of apoptosis. Cytoplasmic vacuolization phenomena and different mitochondrial morphological changes can be appreciated. The most evident one is the increase of electron density (yellow arrow) that may correspond to changes of mitochondrial membrane potential (Pellegrini et al., 2007). Interestingly, in some cases mitochondria elongated (white arrow), probably to maintain ATP production (Gomes et al., 2011), allowing survival of cells in oxidative environments (due to PMA addition). After three additional hours, more prominent events of apoptosis and autophagy were detected as can be noticed by the accumulation of double-membraned cytoplasmic vacuoles containing organelles or cellular debris (yellow star). At 1 h post-infection, *M. catarrhalis* bacterial cells were internalized in a single membrane vesicle, showing a well-preserved ultrastructure. After three additional hours, cells were packed with an increased number of bacterial cells present in larger vesicles. Despite an evident suffering state induced by PMA-addition, the morphology of infected and uninfected host cells was almost the same as they had not perceived the presence of bacterial cells. Conversely, at 1 h post-infection by NTHi, a small number of bacteria were found to be internalized and phenomena of condensation of the internal mitochondrial cristae were detected. In the last time point, dHL-60 cells infected by NTHi showed marked events of late stages of apoptosis (white arrow) and autophagosomes containing cellular debris. The few internalized NTHi bacterial cells were present in double-membraned autophagic vacuoles (yellow arrow) indicating that neutrophil-like cells were active in the clearance of NTHi infections.

Further investigations on the survival of internalized bacteria and their interplays in neutrophil-like cells were carried out by counting survived bacteria in the same experimental condition reported in Figure 5A. ROS-induced dHL-60 cells were infected with *M. catarrhalis* or NTHi at MOI 50 (single infection, red and blue bars in Figure 5, respectively), or co-infected with both the bacteria (MOI 50 each bacterium, black and gray bars, respectively) (Figure 5D). The intracellular survival of bacteria over time was determined by dividing the CFU/ml obtained at 4 h to that recorded at 1 h (ratio 4 h/1 h), as it is shown in Table 1. In the single infection system, *M. catarrhalis* overcame the antimicrobial effect of chemically induced ROS, surviving over 4 h of post-infection. In fact, the number of bacterial cells slightly increased (Figure 5D, red bars).On the contrary, the viability of NTHi dramatically decreased (Table 1, blue bars). In summary, the recorded ratios 4 h/1 h were 1.5 and 0.2 for *M. catarrhalis* and NTHi, respectively (Table 1). This data indicated that NTHi was highly susceptible to ROS generation being efficiently killed by these immune cells. In the co-infection system, the viability of *M. catarrhalis* bacterial cells remained unchanged compared to that observed in single infection (Figure 5D, black and red bars, respectively), suggesting that the presence of NTHi had no influence on *M. catarrhalis* capability to tackle the antimicrobial action of ROS production. In fact, ratio 4 h/1 h was 1.6 and the observed CFU/ml at both time points were similar in the two experimental conditions (single and co-infection). Interestingly, in the co-infection, the drastic reduction of NTHi viability was not observed (Figure 5D, gray bars). The recorded ratio 4 h/1 h was 0.8 (Table 1), indicating that the presence of *M. catarrhalis* reduced the killing of NTHi by chemically activated dHL-60 cells, thus providing benefit of survival (ratio 4 h/1 h 0.8 and 0.2 in the co-infection and single infection, respectively), (Table 1). However, the strategies exploited by *M. catarrhalis* to survive or even proliferate after internalization and how it may affect NTHi internalization and its viability in an oxidative-like environment remain to be fully elucidated.

Human opsonins increase Mcat and NTHi neutrophil uptake without affecting their ROS response

Upon entry into the human host, bacteria are exposed to immune mediators (complement and immunoglobulins) that can coat to the bacterial surface opsonizing them. Apart from the opsonin-independent uptake mediated by CEACAM-3 receptor (Buntru et al., 2011), opsonization leads to enhanced neutrophil recognition and

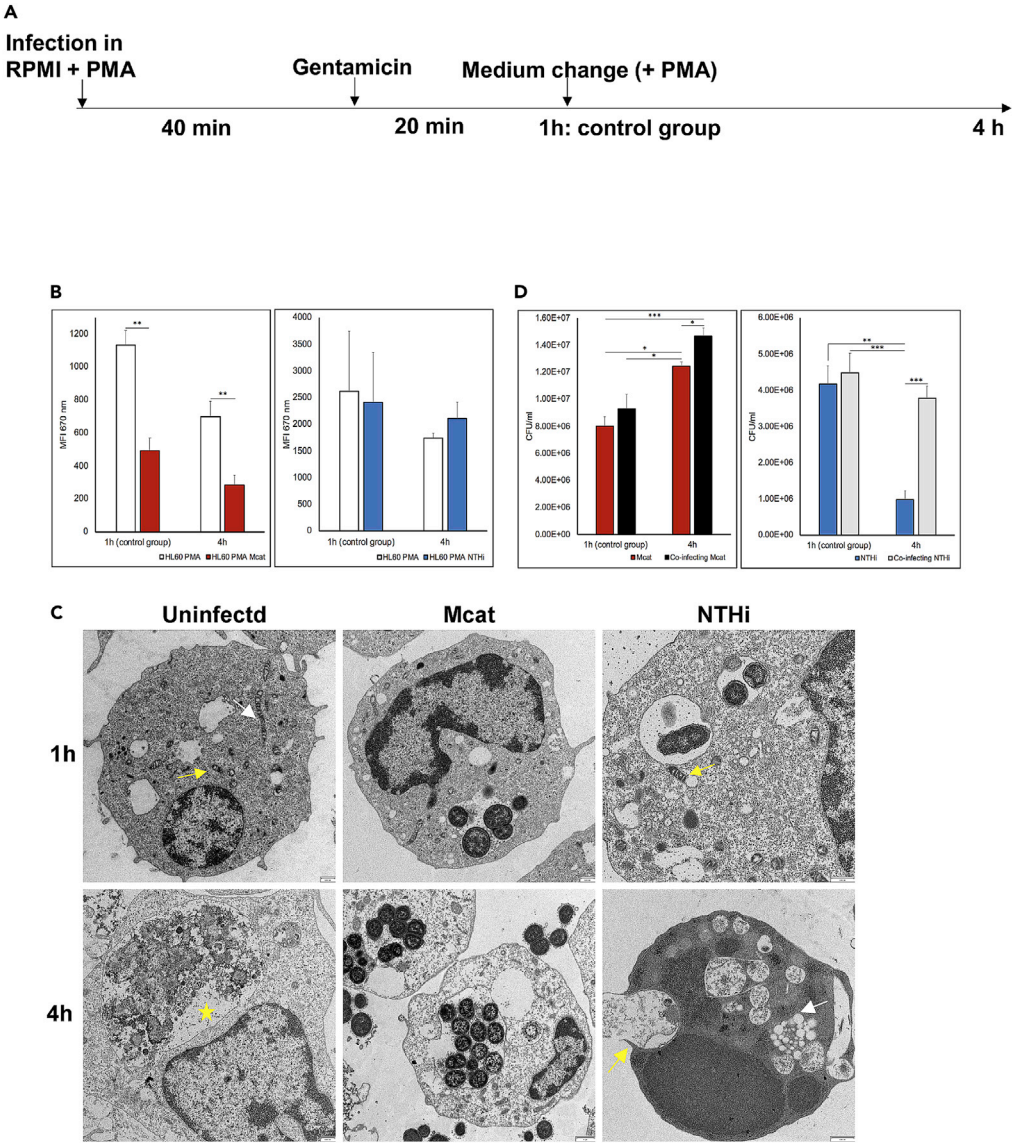

Figure 5. *M. catarrhalis* interferes with the autophagic pathway surviving intracellularly and reducing the killing of NTHi

ROS-stimulated dHL-60 cells were non-infected (black bars) or incubated with *M. catarrhalis* or NTHi individually or in their combination at MOI 50 for 40 min. Then non adherent bacteria were washed out and gentamicin was added for 20 min to inhibit growth of extracellular bacteria. From this time (1 h, control group), samples were incubated for additional 3 h (for a total of 4 h).

(A) Schematic representation of the "autophagic response and intracellular survival assay".

(B) The autophagic response was monitored by flow cytometry using the LC3-II as a marker. The mean fluorescence intensity (MFI) at 670 nm was determined without performing gates. The resulting graph is obtained from four independent experiments. ROS-stimulated dHL-60 cells were non-infected (black bars) or incubated with *M. catarrhalis* (striped bars) or NTHi (green bars) Bars represent means ±SE *$p < 0.05$; **$p < 0.01$.

(C) Transmission electron microscopy on uninfected ROS-induced dHL60 cells (left panels) and infected by non-opsonised *M. catarrhalis* at MOI 50 (middle panels) or by non-opsonised NTHi 658 at MOI 50 (right panels). Scale bars, 500 nm.

(D) By using the protocol whose schematic representation is reported in panel (A), chemically-activated cells were infected by only *M. catarrhalis* (red bars) and NTHi (blue bars) at MOI 50 (single infection), or with both the bacteria (co-infection with MOI 50 each bacterium, black and gray bars). By dilution plating onto BHI or HAE2 plates, the number of colonies obtained per condition was calculated to plot CFU/ml and to determine the survival of *M. catarrhalis* and NTHi, respectively. Bars represent means ± SE. MFI, Mean fluorescence intensity. *$p < 0.05$; **$p < 0.01$; ***$p < 0.001$

Table 1. Bacterial intracellular survival in dHL-60 cells

ROS-induced dHL-60 cells

	1 h (CFU/ml)	4 h (CFU/ml)	Ratio 4 h/ 1 h
Mcat	8.01E+06	1.24E+07	1.5
Co-infecting Mcat	9.26E+06	1.46E+07	1.6
NTHi	4.16E+06	9.88E+05	0.2
Co-infecting NTHi	4.49E+06	3.78E+06	0.8

Table reporting the CFU/ml obtained at 1 and 4 h post-infection for *M. catarrhalis* and NTHi both in sigle and co-infection. Bacterial intracellular survival was determined by dividing the CFU/ml obtained at 4 h to that recorded at 1 h (ratio 4 h/1 h).

phagocytosis of bacterial pathogens, mediated by Fcg receptors (FcgR) (Theprungsirikul et al., 2021). Hence, we decided to evaluate the effect of Mcat and NTHi opsonization on the uptake and intracellular ROS production in dHL-60 cells. Tre human sera were pooled and used as complement source at 10% (hereafter called normal human sera, NHS). By flow cytometry, we showed that more than 90% of NHS-treated Mcat and NTHi bacterial populations have C3b and human immunoglobulins coated on their surface without loss of viability (Figure S4). At 2 h post-infection, compared to unopsonized bacteria, opsonization of Mcat and NTHi significantly enhanced bacterial uptake by dHL-60 cells (3.6- and 2- fold increase, respectively), delineating the importance of complement and immunoglobulins in increasing internalization (Figure 6A). As described above, intracellular ROS generation was evaluated 2 h post-infection. As can be observed in Figure 6B, opsonized Mcat still induced less ROS production in nonstimulated dHL-60 cells compared to NTHi (Figure 6B) and was able to actively interfere with this response in PMA-activated cells while NTHi did not (Figure 6C). Curiously, for both Mcat and NTHi, the uptake of opsonized bacteria by dHL-60 cells lead to lower ROS production compared to their non-opsonized counterparts. Serum opsonins are thus important for increasing Mcat and NTHi neutrophil uptake while only slightly affecting ROS generation.

Mcat and NTHi behaviors in primary cells strongly reflect those observed in dHL-60 cells

Lastly, to verify if our main findings relate to primary cells, human polymorphic nuclear leukocytes (PMNs) isolated from whole blood were used. We challenged PMNs from 7 different donors (with or without PMA activation) with non-opsonized *M. catarrhalis* or NTHi (MOI 50) and measured the intracellular ROS production by flow cytometry at 2 h post-infection, using CellRox. Later time points were not considered as PMA strongly affected the viability of host cells. As shown in Figure 7A, NTHi induced a stronger oxidative stress response in unstimulated PMNs compared to Mcat. Moreover, Mcat dampened ROS production in PMA-activated PMNs while NTHi did not (Figure 7B). Survival of internalized bacteria was determined by enumeration of CFU after infection of PMA-activated PMNs with Mcat or NTHi at MOI 50 (single infection, red and gray spots, respectively), or co-infected with both the bacteria (MOI 50 each bacterium, black and blue spots, respectively) (Figure 7C). In the single infection system, more Mcat bacteria were able to survive compared to NTHi. In the co-infection system, the presence of *M. catarrhalis* showed a strong trend for lowered killing of NTHi by chemically activated cells, resulting in a survival ratio of co-infection/single infection of 3.3 (Figure 7C and Table 2). This suggests that also in PMNs, Mcat co-infection provides a more favourable niche for NTHi survival likely through downregulation of ROS and the oxidative stress-related responses.

Visualization of NET structures was performed by SEM (Figure 7D) and confocal microscopy (Figure 7E). The extracellular traps were clearly visible in PMA-activated primary cells and non-stimulated cells infected by NTHi. In single infection, NTHi was surrounded by these web-like structures but in co-infection system, NETosis was visibly lower. Of interest, a lower amount of extracellular fibers were present in the case of Mcat-infecting PMA-activated cells compared to Mcat-infecting unstimulated neutrophils. Moreover, in the latter case, less internalization and more grape-like structures of adherent bacteria were present. From the above data, we conclude that NTHi elicits prominent NETosis events in infected cells while *M. catarrhalis* is able to dampen NET generation in PMA-stimulated cells or cells infected by NTHi. Therefore, the key results obtained with dHL-60 cells were confirmed by using primary cells, suggesting that the observed phenotypes were not strictly related to the used cell line.

DISCUSSION

The relationship between dysbiosis of lung microbiome and COPD have been investigated in many studies reporting a relevant increase in nontypeable *H. influenzae* (NTHi) and *M. catarrhalis* (Mcat) bacterial

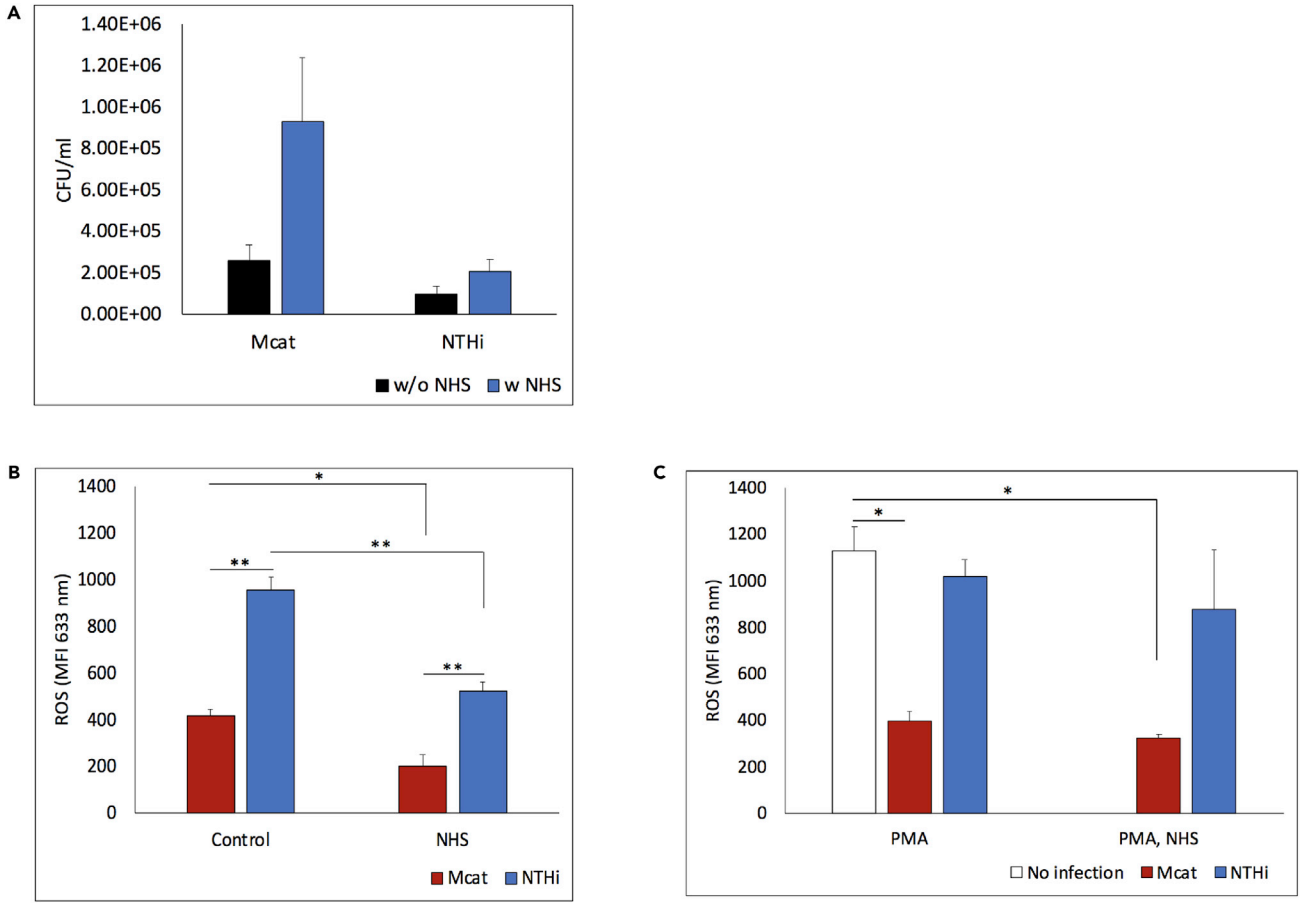

Figure 6. Human opsonins increase Mcat and NTHi neutrophil uptake without affecting their ROS response

Exponentially growing Mcat and NTHi bacteria were left unopsonized or treated with 10% of human sera, hereafter called NHS. dHL-60 cells were challenged for 2 h with unopsonized or opsonized Mcat or NTHi at MOI 50.

(A) By dilution plating onto BHI or HAE2 plates, the number of colonies obtained per condition was calculated to plot CFU/ml and to determine the phagocytic uptake of *M. catarrhalis* and NTHi, respectively.

(B and C) (B) Nonstimulated and (C) PMA-activated dHL60 cells were infected with *M. catarrhalis* BBH18 (red bars) or NTHi 658 (blue) at MOI 50 and ROS production at 2h post-infection was monitored using CellRox (intracellular ROS). MFI at 633 nm from at least three independent experiments at the indicated time point after infection was determined by flow cytometry. Bars represent means ± SE. MFI, Mean fluorescence intensity. *p < 0.05

detection during exacerbations (Mayhew et al., 2018). COPD is a progressive disease characterized by neutrophilic inflammation, a condition known to promote the excessive formation of ROS and ROS-related responses such as neutrophil extracellular traps (NETs) and autophagy (Glasauer and Chandel, 2013).

Here, we investigated the interaction *in vitro* of NTHi and M. catarrhalis with neutrophil-like dHL-60 cells. We have shown that both bacteria are internalized in an opsoninin-independent manner. These findings are consistent with the report of Schmitter et al. (2004), demonstrating that granulocytes can recognize these two human adapted Gram-negative bacteria in an opsonin-independent manner via bacterial binding to CEACAM3 receptor (Schmitter et al., 2004). However, in this study, we observed that the percentage of non-infected cells is by far higher in NTHi infections and few bacterial cells are internalized. By contrast, *M.catarrhalis* is readily phagocytosed, is not killed and internalized bacterial numbers accumulate over time.

We found that both bacteria can induce levels of ROS compared to non-stimulated dHL-60 cells, albeit Mcat to significantly lower levels than NTHi. Our data confirm the findings of Heinrich et al. who found evidences that *M. catarrhalis* UspA1 engagement of CEACAM3 granulocytes receptors induce ROS production (Heinrich et al., 2016) and those showing NTHi being able to induce oxidative stress (Essilfie et al., 2011)

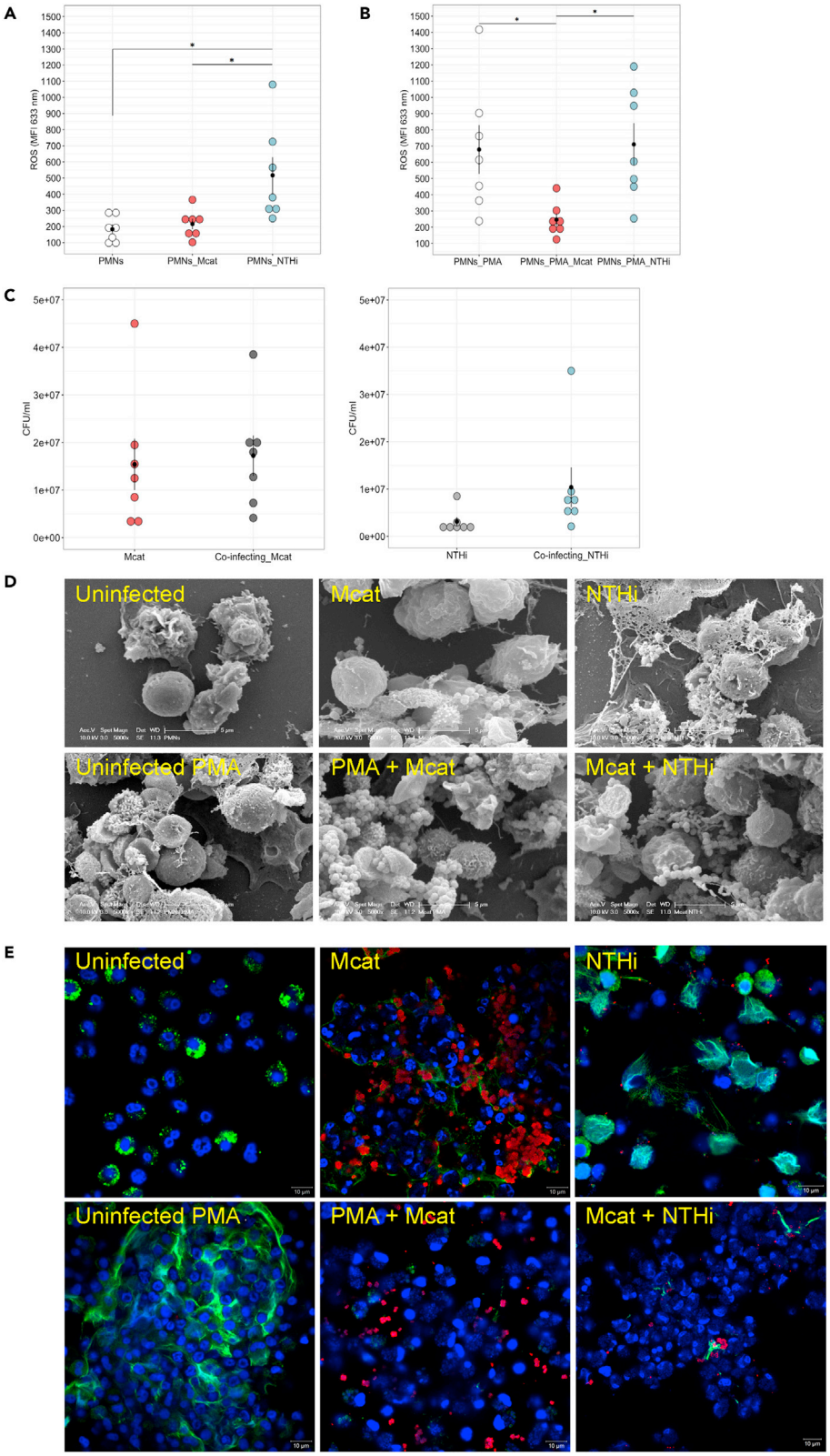
A
ROS (MFI 633 nm)
PMNs
PMNs_Mcat
PMNs_NTHi
B
ROS (MFI 633 nm)
PMNs_PMA
PMNs_PMA_Mcat
PMNs_PMA_NTHi
C
CFU/ml
Mcat
Co-infecting_Mcat
CFU/ml
NTHi
Co-infecting_NTHi
D
Uninfected
Mcat
NTHi
Uninfected PMA
PMA + Mcat
Mcat + NTHi
E
Uninfected
Mcat
NTHi
Uninfected PMA
PMA + Mcat
Mcat + NTHi

Figure 7. Mcat and NTHi behaviors in primary cells strongly reflect those observed in dHL-60 cells

(A and B) PMNs (A) unstimulated or (B) PMA-activated were left uninfected (white spots) or infected with the *M. catarrhalis* BBH18 (red spots) or NTHi 658 (blue spots) at MOI 50 and ROS production at 2 h post-infection was monitored using CellRox (intracellular ROS). MFI at 633 nm from seven donors was determined by flow cytometry. Bars represent means ± SE. MFI, Mean fluorescence intensity. The MFI obtain for each donor is represented by a spot. *p < 0.05.

(C) PMNs were infected by only *M. catarrhalis* (red bars) or NTHi (blue bars) at MOI 50 (single infection), or with both the bacteria (co-infection with MOI 50 each bacterium, black and gray bars). By dilution plating onto BHI or HAE2 plates, the number of colonies obtained per condition was calculated to plot CFU/ml and to determine the microbial interplay (ratio co/single infection) of *M. catarrhalis* and NTHi, respectively. Bars represent means ± SE and the CFU/ml obtained for each donor is represented by a spot.

(D and E) Visualization of NET structures. (D) Samples were fixed and analyzed by scanning electron microscopy. (E) Samples were fixed and stained for DNA (blue), myeloperoxidase (green) and adherent bacteria (red). Bacteria were detected by staining for UspA2 (rabbit polyclonal antibodies) and for whole bacteria for *M. catarrhalis* and NTHi, respectively. The stained cells were analyzed by immunofluorescence microscopy. Scale bars, 10 μm

both in the lungs of BALB/c mice intratracheally inhaled with this bacterium (King et al., 2015) and in a tissue culture model (Kalograiaki et al., 2016). However, despite the higher extent of uptake of *M. catarrhalis* by the dHL-60 cells with respect to NTHi, we observed that the oxidative stress response induced by *M. catarrhalis* was far lower than that of NTHi, suggesting that M. catarrhalis suppresses the oxidative burst. Additionally, as in COPD neutrophils are described aberrant due to abnormally high ROS generation, degranulation, phagocytosis and NET production (Stockley et al., 2013), the oxidative burst was also evaluated in chemically-activated cells. We demonstrated for the first time that these neutrophil-like cells are impaired to respond to chemical activation by PMA when infected by *M. catarrhalis* but not by NTHi. Therefore, contrary to other pathogenic bacteria such as *Staphylococcus aureus* (Beavers and Skaar, 2016) and similarly to group A *Streptococcus* (Uchiyama et al., 2015), *M. catarrhalis* actively interferes with extracellular and intracellular oxidative stress response even in the presence of a strong stimulus such as PMA. Interestingly, in the presence of opsonins through the addition of human serum as antibody and complement source, despite an expected significant increase in bacterial uptake for both bacteria, the ability of Mcat to dampen ROS response was maintained suggesting this phenotype is opsonin-independent.We also showed that the observed phenotype was confirmed in primary neutrophils. In contrast to NTHI, Mcat infection dampened ROS production in activated PMNs, while no significant ROS was measured after infection of unstimulated PMNs. Therefore, an in-depth analysis of the mechanisms exploited by *M. catarrhalis* to contrast ROS production was pursued. It was demonstrated that the reduction of the respiratory burst was contact-dependent, phagocytosis-independent and not related to the secretion of effector proteins or toxins. Similarly, it has been reported that *Chlamydia* interferes with chemical-mediated activation of neutrophils. However, the impairment of ROS generation by *Chlamydia* is accomplished by secreted protease-like activating factor (CPAF), which is responsible for the cleavage of formyl peptide receptor 2 (FPR2), an immune-activating receptor (Rajeeve et al., 2018). As direct contact of *M. catarrhalis* to neutrophil-like cells is required for suppression of ROS generation, we evaluated the ability of *M. catarrhalis* to bind to a number of immunosuppressive receptors such as Sialic acid-binding immunoglobulin-type lectins (Siglecs) which have been shown to modulate oxidative stress responses (Schwarz et al., 2015). By engaging the inhibitory Siglec-9 and Siglec-5 human neutrophils' receptors, bacteria such as group B *Streptococcus* and *P. aeruginosa* are able to impair oxidative burst and NET formation (Carlin et al., 2009) (Khatua et al., 2012). Flow cytometry experiments demonstrated that *M. catarrhalis* can bind both Siglec-5 and Siglec-9 receptors, highlighting these as possible candidates as interactors leading to the suppression observed.

NETs represent an important hallmark in COPD and are related to ROS release. NETs trap, neutralize and kill bacteria and are thought to prevent bacterial dissemination (Delgado-Rizo et al., 2017). As a matter of fact, bacteria with mutations in NET-degrading nucleases (Juneau et al., 2015) or in capsule genes (Wartha et al., 2007) are impaired in their ability to disseminate, increasing their NET trapping *in vitro* (Papayannopoulos, 2018). By using both quantitative and qualitative approaches, we demonstrated that *M. catarrhalis* not only induces NET generation in infected cells to a lesser extent compared to NTHi, but it is able to suppress this response in PMA-stimulated cells and cells co-infected by NTHi. NTHi has already been shown to induce high oxidative stress and NETs formation both in the lungs of BALB/c mice (King et al., 2015), in a tissue culture model (Kalograiaki et al., 2016) and to exploit NETs structures for its survival in the middle ear (Juneau et al., 2011). It has recently been hypothesized that NTHi uses a phase variable mechanism to evade and/or to survive within NET (Robledo-Avila et al., 2020). Thus, it is presumable that prevalent phase-variation occurring in the NTHi strain used in this study induces a prominent neutrophil extracellular

Table 2. Mcat and NTHi microbial interplays in primary cells

Primary cells, PMNs		
	2 h (CFU/ml)	Ratio co/single infection
Mcat	1.54E+07	
Co-infecting Mcat	1.72E+07	1.1
NTHi	3.13E+06	
Co-infecting NTHi	1.04E+07	3.3

Tablereporting the CFU/ml obtained at 2 h post-infection for *M. catarrhalis* and NTHi both in sigle and co-infection. The microbial interplay was determined by dividing the CFU/ml obtained in co-infection to that recorded in single infection (ratio co/single infection).

trap response, leading to the significant killing of the bacterium. Similarly to NTHi, the pore-forming toxin leuko-toxin GH of *S. aureus* is sufficient to drive NETosis (Malachowa et al., 2013). Furthermore, a very recent study has shown that neutrophils may assist macrophages in the clearance of *S. aureus* infection through NET structures (Monteith et al., 2021). By considering the aforementioned examples, it would be interesting to evaluate not only the role of Mcat nucleases but also the cooperation between neutrophils and mature macrophages rather than isolated innate immune cells in the bacterial response to NET formation.

The last innate immunological response that was investigated is autophagy, a process that maintains cellular homeostatic functions and is also used against microbes, including the selective delivery of microorganisms to degradative lysosomes (a process referred to to as xenophagy) (Levine and Kroemer, 2008; Jo et al., 2013). By controlling bacterial replication, autophagy plays an important role in activation of innate and adaptive immunity (Lamark et al., 2009). Generally, successful intracellular pathogens may antagonize both the signaling pathways that activate autophagy as well as the membrane trafficking events required for lysosomal delivery and degradation. This is the case of *Mycobacterium tuberculosis*, a bacterium able to interfere with phagolysosome biogenesis (Gutierrez et al., 2004) and whose lipoprotein LprE suppresses autophagic response to enhance bacterial survival in macrophages (Padhi et al., 2019). By contrary, numerous medically important pathogens, including *Salmonella enterica*, are degraded *in vitro* by xenophagy (Wild et al., 2011). Here, it is shown that *M. catarrhalis* is able to interfere with the autophagic pathway of dHL-60 cells while NTHi does not, as demonstrated by the expression levels of the LC3-II marker. These observations were supported byEM analysis of cells infected by single bacterium. In fact, the number of *M. catarrhalis* bacterial cells increases over 4 h post-infection. In addition, uninfected cells or cells containing internalized *M. catarrhalis* showed a similar morphology, indicating that *M. catarrhalis* had no influence on host viability. More evident phenomena of apoptosis (as apoptoticbodies formation) were detected when cells were infected by NTHi. Through inhibiting autophagy, *M. catarrhalis* may provide itself with an intracellular niche where apoptosis is delayed, and the bacteria survive by evading the phagolysosomes. However, how Mcat survives inside the host cells and antagonizes autophagy remains to be cleared. We can only speculate that it may occur through different strategies: by interfering with the a) signaling pathways that activate autophagy as well as b) the membrane trafficking events required for lysosomal delivery or c) by directly targeting mitochondria-associated ER membranes (MAMs, where autophagosomes are formed) (Escoll et al., 2016).

Indeed, by bacterial cell counting, we have shown that dHL-60 cells failed to eliminate *M. catarrhalis*, suggesting a clear capability to subvert and exploit the host innate immune responses to support its replicative life cycle. Thus, neutrophil-like cells are a target of *M. catarrhalis* infection, providing a replicative niche. By contrast, NTHi seems to be highly sensitive to the antimicrobial arsenal mounted by neutrophil-like cells with ROS and likely NETs and autophagy playing a strong bactericidal effect. Another interesting finding of this study is the observation that in PMA-stimulated cells *M. catarrhalis* provided a benefit of survival for the co-infecting bacterium, protecting NTHi from oxidative stress and NETosis and favoring its persistence in neutrophil-like cells. Even if a unique time point was considered, Mcat-infecting PMNs remarkably enhanced NTHi survival compared to a single infection (fold increase of 3.3). Interestingly, all these microbial interplays closely resemble those occurring between *C. trachomatis* and *N. gonorrhoeae* in the urogenital tract in which the former is able to provide a safer niche for the co-infecting bacterium. Nevertheless, the mechanisms by which *M. catarrhalis* reprograms

the antimicrobial responses of these innate immune cells to survive and enhance NTHi internalization and viability remain to be unraveled.

Altogether, we have set up an *in vitro* model that reproduces the oxidative environment that bacterial pathogens encounter in the host and provided a framework to begin the understanding of how *M. catarrhalis* and NTHi face the lung oxidative environments. We have revealed that *M. catarrhalis* suppresses efficient innate immune responses acting on several defense mechanisms such as ROS, NETosis, autophagy and phagocytic killing through an unknown contact dependent mechanism. In co-infection, *M. catarrhalis* protects NTHi from the activated phagocytic cell responses that may be active in the common anatomical sites. In fact, other studies have reported synergies between these two pathogens that colonise very similar niches such as the nasopharynx and middle ears (Lee et al., 2020; Yamanaka et al., 2008). Of interest, pneumococcus produces millimolar amounts of H_2O_2 able to reduce viability of competing bacteria (Pericone et al., 2000). This is particularly true for NTHi (Johnson et al., 2015; Wypych et al., 2019). By contrast, Weiser and colleagues indicated that *M. catarrhalis* was highly resistant to exogenous oxidative stress compared to the co-infecting pathogen *Streptococcus pneumoniae* and *H. influenzae* (Pericone et al., 2000; Hoopman et al., 2011), even if the underlying mechanisms are currently not well defined. Moreover, Mcat releases outer membrane vesicles (OMV), enriched with beta-lactamase and complement resistance factors, act distally providing a safer niche for pathogens such as NTHi and *S. pneumoniae* that reside in the same anatomical sites and that would otherwise be susceptible to beta-lactam antibiotics and host innate immune factors (Schaar et al., 2011; Tan et al., 2007).To conclude, all the research works done so far suggest that even if it was initially considered a commensal, Mcat is actually a harmful co-pathogen (Barker et al., 2015, D'anna et al., 2020). Therefore, an in-depth understanding of the strategies that *M. catarrhalis* utilizes to evade the host's innate immune responses and sustain NTHi infection could suggest prophylactic and therapeutic interventions to tackle COPD and potentially other diseases such as acute otitis media.

Limitations of the study

One of the limitations of this study is the use of only one Mcat and NTHi strains even if these are representative of the COPD disease at exacerbation states. We think that it would be interesting to use other bacterial strains frequently associated with not only COPD but to other respiratory infections including otitis media. In the context of bacterial interplays, another point is the evaluation of *S. pneumoniae* (Spn), the other major pathogens of COPD exacerbations. It has already been shown that through production of ROS, Spn interferes with NTHi colonization whileMcat survival is not affected. Thus, considering the interplays between Mcat, NTHI and Spn, in the human host such as in activated neutrophils, investigating how they respond to ROS production, survive once internalized and how they interact in co-infections, influencing each other, will put the findings into broader context. Moreover, while the phenotypes on the host side were identified, the specific bacterial determinats and host-bacterial interactions involved in these observations remain to be elucidated. We did not determine the bacterial components that interact with either of the tested immunosuppressive Siglec receptors. Regarding the bacterial response to NET formation, it would be worth unraveling the role of Mcat nucleases and the cooperation between neutrophils with mature macrophages rather than a single type of innate immune cells. For the autophagic pathway, it remains to be fully elucidated how Mcat antagonizes autophagy. We can only hypothesize that it occur through a number of strategies: by blocking a) the signaling pathways that activate autophagy, b) the membrane trafficking events (phusion of phagosomes with lysosomes) or c) by directly targeting MAMs. Therefore, understanding the specifics of these interactions is necessary both from bacterial and innate immunology perspectives.

STAR★METHODS

Detailed methods are provided in the online version of this paper and include the following:

- KEY RESOURCES TABLE
- RESOURCE AVAILABILITY
  - Lead contact
  - Material availability
  - Data and code availability
- EXPERIMENTAL MODEL AND SUBJECT DETAILS
  - Cell culture and differentiation
  - Bacterial strains and cultures

SUPPLEMENTAL INFORMATION

Supplemental information can be found online at https://doi.org/10.1016/j.isci.2022.103931.

ACKNOWLEDGMENTS

This work was sponsored by GlaxoSmithKline Biologicals. We thank Mariagrazia Pizza for critically reading the manuscript, Francesca Schiavetti for the help in having access to venous blood, Sara Tomei and Alessia Biolchi for the gift of the three human sera.

AUTHOR CONTRIBUTIONS

Conceptualization, S.N., and C.B; Methodology, S.N., F.G., S.C., S.U.L.and S.T.; Resources, I.D.; Funding Acquisition, I.D.; Writing– Original Draft, S.N., M.M., V.S., C.B.,; Writing–Review and Editing, S.N., S.C., E.F., I.F., S.R.P., M.M, I.D, V.S., D.M., C.B.,; Supervision, V.S., D.M., C.B.

DECLARATION OF INTERESTS

All authors have declared the following interests: S.N and S.C. participate in a post graduate studentship program at GSK; F.G., S.T., E.F., I.F., S.R.P., I.D., D.M. and C.B. are employees of the GSK group of companies; M.M. is a consultant for GSK, Italy.

Received: July 20, 2021
Revised: December 20, 2021
Accepted: February 10, 2022
Published: March 18, 2022

REFERENCES

Aratani, Y. (2018). Myeloperoxidase: its role for host defense, inflammation, and neutrophil function. Arch. Biochem.Biophys. *640*, 47–52.

Barker, B.L., Haldar, K., Patel, H., Pavord, I.D., Barer, M.R., Brightling, C.E., and Bafadhel, M. (2015). Association between pathogens detected using quantitative polymerase chain reaction with airway inflammation in COPD at stable state and exacerbations. Chest *147*, 46–55.

Beavers, W.N., and Skaar, E.P. (2016). Neutrophil-generated oxidative stress and protein damage in Staphylococcus aureus. Pathog. Dis. *74*, ftw060.

Bonsignore, P., Kuiper, J.W.P., Adrian, J., Goob, G., and Hauck, C.R. (2019). CEACAM3-A Prim(at)e Invention for Opsonin-Independent Phagocytosis of Bacteria. FrontImmunol. *10*, 3160.

Brooks, M.J., Sedillo, J.L., Wagner, N., Wang, W., Attia, A.S., Wong, H., Laurence, C.A., Hansen, E.J., and Gray-Owen, S.D. (2008). Moraxella catarrhalis binding to host cellular receptors is mediated by sequence-specific determinants not conserved among all UspA1 protein variants. Infect Immun. *76*, 5322–5329.

Brown, P.J. (2018). The ravages of COPD. Lancet Respir. Med. *6*. https://doi.org/10.1016/S2213-2600(18)30153-X.

Buntru, A., Kopp, K., Voges, M., Frank, R., Bachmann, V., and Hauck, C.R. (2011). Phosphatidylinositol 3'-kinase activity is critical for initiating the oxidative burst and bacterial destruction during CEACAM3-mediated phagocytosis. J. Biol. Chem. *286*, 9555–9566.

Carlin, A.F., Chang, Y.C., Areschoug, T., Lindahl, G., Hurtado-Ziola, N., King, C.C., Varki, A., and Nizet, V. (2009). Group B Streptococcus suppression of phagocyte functions by protein-mediated engagement of human Siglec-5. J. Exp. Med. *206*, 1691–1699.

Choudhury, G., and Macnee, W. (2017). Role of inflammation and oxidative stress in the pathology of ageing in COPD: potential therapeutic interventions. COPD *14*, 122–135.

D'anna, S.E., Maniscalco, M., Cappello, F., Carone, M., Motta, A., Balbi, B., Ricciardolo, F.L.M., Caramori, G., and Stefano, A.D. (2020). Bacterial and viral infections and related inflammatory responses in chronic obstructive pulmonary disease. Ann. Med. *53*, 135–150.

Dan Dunn, J., Alvarez, L.A., Zhang, X., and Soldati, T. (2015). Reactive oxygen species and mitochondria: a nexus of cellular homeostasis. Redox Biol. *6*, 472–485.

De Vries, S.P., Van Hijum, S.A., Schueler, W., Riesbeck, K., Hays, J.P., Hermans, P.W., and Bootsma, H.J. (2010). Genome analysis of Moraxella catarrhalis strain BBH18, [corrected] a human respiratory tract pathogen. J. Bacteriol. *192*, 3574–3583.

Decramer, M., Janssens, W., and Miravitlles, M. (2012). Chronic obstructive pulmonary disease. Lancet *379*, 1341–1351.

Delgado-Rizo, V., Martinez-Guzman, M.A., Iniguez-Gutierrez, L., Garcia-Orozco, A., Alvarado-Navarro, A., and Fafutis-Morris, M. (2017). Neutrophil extracellular traps and its implications in inflammation: an overview. FrontImmunol. *8*, 81.

Deretic, V., Saitoh, T., and Akira, S. (2013). Autophagy in infection, inflammation and immunity. Nat. Rev. Immunol. *13*, 722–737.

Di Stefano, A., Caramori, G., Ricciardolo, F.L., Capelli, A., Adcock, I.M., and Donner, C.F. (2004). Cellular and molecular mechanisms in chronic obstructive pulmonary disease: an overview. Clin. Exp. Allergy *34*, 1156–1167.

Dupre-Crochet, S., Erard, M., and Nubetae, O. (2013). ROS production in phagocytes: why, when, and where? J. Leukoc. Biol. *94*, 657–670.

El-Benna, J., Dang, P.M., Gougerot-Pocidalo, M.A., Marie, J.C., and Braut-Boucher, F. (2009). p47phox, the phagocyte NADPH oxidase/NOX2 organizer: structure, phosphorylation and implication in diseases. Exp. Mol. Med. *41*, 217–225.

Escoll, P., Rolando, M., and Buchrieser, C. (2016). Modulation of host autophagy during bacterial infection: sabotaging host munitions for pathogen nutrition. FrontImmunol. *7*, 81.

Essilfie, A.T., Simpson, J.L., Horvat, J.C., Preston, J.A., Dunkley, M.L., Foster, P.S., Gibson, P.G., and Hansbro, P.M. (2011). Haemophilus influenzae infection drives IL-17-mediated neutrophilic allergic airways disease. PLoS Pathog. *7*, e1002244.

Footitt, J., Mallia, P., Durham, A.L., Ho, W.E., Trujillo-Torralbo, M.B., Telcian, A.G., Del Rosario, A., Chang, C., Peh, H.Y., Kebadze, T., et al. (2016). Oxidative and nitrosative stress and histone deacetylase-2 activity in exacerbations of COPD. Chest *149*, 62–73.

Futosi, K., Fodor, S., and Mocsai, A. (2013). Neutrophil cell surface receptors and their intracellular signal transduction pathways. Int. Immunopharmacol. *17*, 638–650.

Glasauer, A., and Chandel, N.S. (2013). Ros. Curr. Biol. *23*, R100–R102.

Gomes, L.C., Di Benedetto, G., and Scorrano, L. (2011). During autophagy mitochondria elongate, are spared from degradation and sustain cell viability. Nat.Cell Biol. *13*, 589–598.

Grabcanovic-Musija, F., Obermayer, A., Stoiber, W., Krautgartner, W.D., Steinbacher, P., Winterberg, N., Bathke, A.C., Klappacher, M., and Studnicka, M. (2015). Neutrophil extracellular trap (NET) formation characterises stable and exacerbated COPD and correlates with airflow limitation. Respir. Res. *16*, 59.

Gutierrez, M.G., Master, S.S., Singh, S.B., Taylor, G.A., Colombo, M.I., and Deretic, V. (2004). Autophagy is a defense mechanism inhibiting BCG and Mycobacterium tuberculosis survival in infected macrophages. Cell *119*, 753–766.

Heinrich, A., Heyl, K.A., Klaile, E., Muller, M.M., Klassert, T.E., Wiessner, A., Fischer, K., Schumann, R.R., Seifert, U., Riesbeck, K., et al. (2016). Moraxella catarrhalis induces CEACAM3-Syk-CARD9-dependent activation of human granulocytes. Cell Microbiol. *18*, 1570–1582.

Hoopman, T.C., Liu, W., Joslin, S.N., Pybus, C., Brautigam, C.A., and Hansen, E.J. (2011). Identification of gene products involved in the oxidative stress response of Moraxella catarrhalis. Infect Immun. *79*, 745–755.

Imlay, J.A. (2008). Cellular defenses against superoxide and hydrogen peroxide. Annu. Rev. Biochem. *77*, 755–776.

Jaroenpool, J., Pattanapanyasat, K., Noonin, N., and Prachongsai, I. (2016). Aberrant neutrophil function among heavy smokers and chronic obstructive pulmonary disease patients. Asian Pac. J. Allergy Immunol. *34*, 278–283.

Jo, E.K., Yuk, J.M., Shin, D.M., and Sasakawa, C. (2013). Roles of autophagy in elimination of intracellular bacterial pathogens. Front. Immunol. *4*, 97.

Johnson, M.D., Kehl-Fie, T.E., and Rosch, J.W. (2015). Copper intoxication inhibits aerobic nucleotide synthesis in Streptococcus pneumoniae. Metallomics *7*, 786–794.

Juneau, R.A., Pang, B., Weimer, K.E., Armbruster, C.E., and Swords, W.E. (2011). Nontypeable Haemophilus influenzae initiates formation of neutrophil extracellular traps. Infect Immun. *79*, 431–438.

Juneau, R.A., Stevens, J.S., Apicella, M.A., and Criss, A.K. (2015). A thermonuclease of Neisseria gonorrhoeae enhances bacterial escape from killing by neutrophil extracellular traps. J.Infect Dis. *212*, 316–324.

Kalograiaki, I., Euba, B., Proverbio, D., Campanero-Rhodes, M.A., Aastrup, T., Garmendia, J., and Solis, D. (2016). Combined bacteria microarray and quartz crystal microbalance approach for exploring glycosignatures of nontypeable Haemophilus influenzae and recognition by host lectins. Anal Chem. *88*, 5950–5957.

Khatua, B., Bhattacharya, K., and Mandal, C. (2012). Sialoglycoproteins adsorbed by Pseudomonas aeruginosa facilitate their survival by impeding neutrophil extracellular trap through siglec-9. J. Leukoc. Biol. *91*, 641–655.

King, P.T., Sharma, R., O'sullivan, K., Selemidis, S., Lim, S., Radhakrishna, N., Lo, C., Prasad, J., Callaghan, J., Mclaughlin, P., et al. (2015). Nontypeable Haemophilus influenzae induces sustained lung oxidative stress and protease expression. PLoS One *10*, e0120371.

Lamark, T., Kirkin, V., Dikic, I., and Johansen, T. (2009). NBR1 and p62 as cargo receptors for selective autophagy of ubiquitinated targets. Cell Cycle *8*, 1986–1990.

Lee, J., Kim, K.H., Jo, D.S., Ma, S.H., Kim, J.H., Kim, C.S., Kim, H.M., and Kang, J.H. (2020). A longitudinal hospital-based epidemiology study to assess acute otitis media incidence and nasopharyngeal carriage in Korean children up to 24 months. Hum.Vaccin.Immunother. *16*, 3090–3097.

Levine, B., and Kroemer, G. (2008). Autophagy in the pathogenesis of disease. Cell *132*, 27–42.

Malachowa, N., Kobayashi, S.D., Freedman, B., Dorward, D.W., and Deleo, F.R. (2013). Staphylococcus aureus leukotoxin GH promotes formation of neutrophil extracellular traps. J. Immunol. *191*, 6022–6029.

Marino, E., Caruso, M., Campagna, D., and Polosa, R. (2015). Impact of air quality on lung health: myth or reality? Ther. Adv. Chronic Dis. *6*, 286–298.

Mayhew, D., Devos, N., Lambert, C., Brown, J.R., Clarke, S.C., Kim, V.L., Magid-Slav, M., Miller, B.E., Ostridge, K.K., Patel, R., et al. (2018). Longitudinal profiling of the lung microbiome in the AERIS study demonstrates repeatability of bacterial and eosinophilic COPD exacerbations. Thorax *73*, 422–430.

Mccaffrey, R.L., Schwartz, J.T., Lindemann, S.R., Moreland, J.G., Buchan, B.W., Jones, B.D., and Allen, L.A. (2010). Multiple mechanisms of NADPH oxidase inhibition by type A and type B Francisella tularensis. J. Leukoc. Biol. *88*, 791–805.

Monteith, A.J., Miller, J.M., Maxwell, C.N., Chazin, W.J., and Skaar, E.P. (2021). Neutrophil Extracellular Traps Enhance Macrophage Killing of Bacterial Pathogens. Sci. Adv. *7*, eabj2101.

Naito, K., Yamasaki, K., Yatera, K., Akata, K., Noguchi, S., Kawanami, T., Fukuda, K., Kido, T., Ishimoto, H., and Mukae, H. (2017). Bacteriological incidence in pneumonia patients with pulmonary emphysema: a bacterial floral analysis using the 16S ribosomal RNA gene in bronchoalveolar lavage fluid. Int. J. Chron. Obstruct Pulmon Dis. *12*, 2111–2120.

Nguyen, G.T., Green, E.R., and Mecsas, J. (2017). Neutrophils to the ROScue: mechanisms of NADPH oxidase activation and bacterial resistance. Front. Cell Infect Microbiol. *7*, 373.

Padhi, A., Pattnaik, K., Biswas, M., Jagadeb, M., Behera, A., and Sonawane, A. (2019). Mycobacterium tuberculosis LprE suppresses TLR2-dependent cathelicidin and autophagy expression to enhance bacterial survival in macrophages. J. Immunol. *203*, 2665–2678.

Papayannopoulos, V. (2018). Neutrophil extracellular traps in immunity and disease. Nat. Rev. Immunol. *18*, 134–147.

Pavord, I.D., Jones, P.W., Burgel, P.R., and Rabe, K.F. (2016). Exacerbations of COPD. Int. J. Chron. Obstruct Pulmon Dis. *11*, 21–30, Spec Iss.

Pellegrini, M., Finetti, F., Petronilli, V., Ulivieri, C., Giusti, F., Lupetti, P., Giorgio, M., Pelicci, P.G., Bernardi, P., and Baldari, C.T. (2007). p66SHC promotes T cell apoptosis by inducing mitochondrial dysfunction and impaired Ca2+ homeostasis. Cell Death Differ. *14*, 338–347.

Perez, A.C., and Murphy, T.F. (2019). Potential impact of a Moraxella catarrhalis vaccine in COPD. Vaccine *37*, 5551–5558.

Perez, S., Talens-Visconti, R., Rius-Perez, S., Finamor, I., and Sastre, J. (2017). Redox signaling in the gastrointestinal tract. Free Radic. Biol. Med. *104*, 75–103.

Pericone, C.D., Overweg, K., Hermans, P.W., and Weiser, J.N. (2000). Inhibitory and bactericidal effects of hydrogen peroxide production by Streptococcus pneumoniae on other inhabitants

of the upper respiratory tract. Infect. Immun. *68*, 3990–3997.

Porto, B.N., and Stein, R.T. (2016). Neutrophil extracellular traps in pulmonary diseases: too much of a Good thing? Front. Immunol. *7*, 311.

Pyz, E., Marshall, A.S., Gordon, S., and Brown, G.D. (2006). C-type lectin-like receptors on myeloid cells. Ann. Med. *38*, 242–251.

Rajeeve, K., Das, S., Prusty, B.K., and Rudel, T. (2018). Chlamydia trachomatis paralyses neutrophils to evade the host innate immune response. Nat. Microbiol. *3*, 824–835.

Robledo-Avila, F.H., Ruiz-Rosado, J.D., Partida-Sanchez, S., and Brockman, K.L. (2020). A bacterial epigenetic switch in non-typeable Haemophilus influenzae modifies host immune response during otitis media. Front. Cell Infect. Microbiol. *10*, 512743.

Schaar, V., Nordstrom, T., Morgelin, M., and Riesbeck, K. (2011). Moraxella catarrhalis outer membrane vesicles carry beta-lactamase and promote survival of Streptococcus pneumoniae and Haemophilus influenzae by inactivating amoxicillin. Antimicrob. Agents Chemother. *55*, 3845–3853.

Schmitter, T., Agerer, F., Peterson, L., Munzner, P., and Hauck, C.R. (2004). Granulocyte CEACAM3 is a phagocytic receptor of the innate immune system that mediates recognition and elimination of human-specific pathogens. J. Exp. Med. *199*, 35–46.

Schwarz, F., Pearce, O.M., Wang, X., Samraj, A.N., Laubli, H., Garcia, J.O., Lin, H., Fu, X., Garcia-Bingman, A., Secrest, P., et al. (2015). Siglec receptors impact mammalian lifespan by modulating oxidative stress. Elife *4*, e06184.

Smirnov, A., Daily, K.P., and Criss, A.K. (2014). Assembly of NADPH oxidase in human neutrophils is modulated by the opacity-associated protein expression State of Neisseria gonorrhoeae. Infect Immun. *82*, 1036–1044.

Stockley, J.A., Walton, G.M., Lord, J.M., and Sapey, E. (2013). Aberrant neutrophil functions in stable chronic obstructive pulmonary disease: the neutrophil as an immunotherapeutic target. Int. Immunopharmacol. *17*, 1211–1217.

Tan, T.T., Morgelin, M., Forsgren, A., and Riesbeck, K. (2007). Haemophilus influenzae survival during complement-mediated attacks is promoted by Moraxella catarrhalis outer membrane vesicles. J. Infect. Dis. *195*, 1661–1670.

Theprungsirikul, J., Skopelja-Gardner, S., Wierzbicki, R.M., Sessions, K.J., and Rigby, W.F.C. (2021). Differential enhancement of neutrophil phagocytosis by anti-bactericidal/permeability-increasing protein antibodies. J. Immunol. *207*, 777–783.

Uchiyama, S., Dohrmann, S., Timmer, A.M., Dixit, N., Ghochani, M., Bhandari, T., Timmer, J.C., Sprague, K., Bubeck-Wardenburg, J., Simon, S.I., and Nizet, V. (2015). Streptolysin O rapidly impairs neutrophil oxidative burst and antibacterial responses to group A Streptococcus. Front. Immunol. *6*, 581.

Vareechon, C., Zmina, S.E., Karmakar, M., Pearlman, E., and Rietsch, A. (2017). Pseudomonas aeruginosa effector ExoS inhibits ROS production in human neutrophils. Cell Host Microbe *21*, 611–618.e5.

Wartha, F., Beiter, K., Albiger, B., Fernebro, J., Zychlinsky, A., Normark, S., and Henriques-Normark, B. (2007). Capsule and D-alanylated lipoteichoic acids protect Streptococcus pneumoniae against neutrophil extracellular traps. Cell Microbiol. *9*, 1162–1171.

Wild, P., Farhan, H., Mcewan, D.G., Wagner, S., Rogov, V.V., Brady, N.R., Richter, B., Korac, J., Waidmann, O., Choudhary, C., et al. (2011). Phosphorylation of the autophagy receptor optineurin restricts Salmonella growth. Science *333*, 228–233.

Wypych, T.P., Wickramasinghe, L.C., and Marsland, B.J. (2019). The influence of the microbiome on respiratory health. Nat. Immunol. *20*, 1279–1290.

Yamanaka, N., Hotomi, M., and Billal, D.S. (2008). Clinical bacteriology and immunology in acute otitis media in children. J. Infect. Chemother. *14*, 180–187.

Zeng, M.Y., Miralda, I., Armstrong, C.L., Uriarte, S.M., and Bagaitkar, J. (2019). The roles of NADPH oxidase in modulating neutrophil effector responses. Mol. Oral Microbiol. 27–38.

STAR★METHODS

KEY RESOURCES TABLE

REAGENT or RESOURCE	SOURCE	IDENTIFIER
Antibodies		
Rabbit anti-UspA2	This study	N/A
Rabbit anti total NTHi inactivated	This study	N/A
Alexa Fluor 647 goat anti-rabbit IgG (H+L)	ThermoFisher	Cat# A21245; RRID: AB_2535813
CEACAM1 Recombinant Rabbit Monoclonal Antibody (103)	ThermoFisher	Cat# MA5-29142; RRID:AB_2785064
SIGLEC5/SIGLEC14 Monoclonal Antibody (1A5)	ThermoFisher	Cat# MA5-28140;RRID: AB_2745122
SIGLEC9 Recombinant Rabbit Monoclonal Antibody (8H11L21)	ThermoFisher	Cat #703464; RRID: AB_2811733
Alexa Fluor 488 goat anti-rabbit IgG (H+L)	ThermoFisher	Cat # A32731; RRID: AB_2633280
Myeloperoxidase Monoclonal Antibody (2C7)	ThermoFisher	Cat# MA1-80878; RRID: AB_934783
Alexa Fluor 488 goat anti-mouse IgG (H+L)	ThermoFisher	Cat # A32723; RRID; AB_2633275
LC3B Polyclonal Antibody	ThermoFisher	Cat# PA5-32254; RRID: AB_2549727
FITC-conjugated polyclonal anti-human C3 antibody	ThermoFisher	Cat# PA1-28933; RRID: AB_1954681
Goat anti-Human IgG (H+L) Cross-Adsorbed Secondary Antibody, Alexa Fluor 594	ThermoFisher	Cat# A-11014; RRID: AB_2534081
Goat anti-Rabbit IgG (H+L) Cross-Adsorbed Secondary Antibody, Alexa Fluor 594	ThermoFisher	Cat# A-11012; RRID: AB_2534079
Bacterial and virus strains		
Moraxella catarrhalis BBH18	Kristian Riesbeck	GenBank: GCA_000092265.1
Nontypeable *Haemophilus influenzae* NTHi 658	Mayhew et al., 2018	AERIS Study ID: EPI-HIP 001 BOD UK
Biological samples		
Human sera	ID: 2543,	Phleb001_20180404-AXB-1805_ Phleb001 generic
Human sera	ID: 6002	Phleb001_20180404-AXB-1805_ Phleb001 generic
Human sera	ID: 2151	Phleb001_20180404-AXB-1805_ Phleb001 generic
Whole blood from 7 donors	CHU Tivoli (BELGIUM)	N/a
Chemicals, peptides, and recombinant proteins		
RPMI 1640 medium, GlutaMAX supplement	Gibco	Cat# 61870-010
RPMI 1640 Medium, no phenol red	Gibco	Cat# 11835-030
N,N-Dimetilformammide	Sigma-Aldrich	Cat# D4551
Fetal Bovine Serum, qualified, Brazil	Gibco	Cat# 10270106
Phorbol 1-myristate 13-acetate (PMA)	Sigma-Aldrich	Cat# P8139
Cytochalisin D	Sigma-Aldrich	Cat# C8273
Saponin	Sigma-Aldrich	Cat# 47036
Albumin bovine serum (BSA)	Sigma-Aldrich	Cat# A3059
Brain-Heart Infusion Broth (BHI)	BD Difco	Cat# 237500
Chocolate Haemophilus 2 agar (HAE2)	BioMerieux	Cat# 43681

(*Continued on next page*)

Continued

REAGENT or RESOURCE	SOURCE	IDENTIFIER
Haemin	Sigma-Aldrich	Cat# 51280
Nicotinamide adenine dinucleotide (NAD)	Sigma-Aldrich	Cat# N1511
4% (v/v) formaldehyde	Sigma-Aldrich	Cat# 100496
CellROX Deep Red Reagent	ThermoFisher	Cat# C10422
Aqua fluorescent reactive dye *for 405 nm excitation	ThermoFisher	Cat# L34965A
Luminol	Sigma-Aldrich	Cat# 123072
CEACAM-1 recombinant protein	VWR	Cat# 91-404
Siglec-5 recombinant protein	VWR	Cat# 96-691
Siglec-9 recombinant protein	VWR	Cat# 96-630
HBSS, no calcium, no magnesium, no phenol red	ThermoFisher	Cat# 14175095
Micrococcal Nuclease	ThermoFisher	Cat# EN0181
Ethylenediaminetetraacetic acid (EDTA)	Sigma-Aldrich	Cat# E6758
Calcium Chloride ($CaCl_2$)	Sigma-Aldrich	Cat# C5670
4′,6-Diamidino-2-Phenylindole, Dihydrochloride (DAPI)	ThermoFisher	Cat# D1306
Dulbecco's Phosphate-Buffered Saline (DPBS)(1X)	ThermoFisher	Cat# 14190144
Gentamicin sulfate	Sigma-Aldrich	Cat# G1914
Ethanol absolute anhydrous	Carlo Erba	Cat# 414601
Osmium tetroxide (OsO_4)	Sigma-Aldrich	Cat# 201030
Critical commercial assays		
Quant iT PicoGreen	ThermoFisher	Cat# P11496
Experimental models: Cell lines		
HL-60	ATCC	CCL-240
Quantification and statistical analysis		
ANOVA	R version 3.6.0	https://cran.r-project.org/bin/macosx/
Student's t-tests	R version 3.6.0	https://cran.r-project.org/bin/macosx/

RESOURCE AVAILABILITY

Lead contact

Further information and requests for resources and reagents should be directed to and will be fulfilled by the lead contact, Cecilia Brettoni (cecilia.x.brettoni@gsk.com)

Material availability

This study did not generate new unique reagents.

Data and code availability

- All data reported in this paper will be shared by the lead contact upon request.
- This paper does not report original code.
- Any additional information required to reanalyze the data reported in this paper is available from the lead contact upon request.

EXPERIMENTAL MODEL AND SUBJECT DETAILS

Cell culture and differentiation

The human promyelocytic cell line HL-60 (ATCC CCL-240) was maintained in RPMI 1640 medium, GlutaMAX supplement (ThermoFisher) supplemented with 10% fetal bovine serum (FBS, ThermoFisher) at 37°C and 5% CO2 between 2.0 × 10^5 and 1 × 10^6 cells/ml. 4 × 10^5 cells/ml were differentiated with 100 mM with N, N-dimethylformamide (DMF, Sigma). HL-60 cells are differentiated into granulocytes by 4–5 days of treatment and are ready to be used as phagocytes with a typical yield of 8-12 × 10^5 cells/ml. For all host-pathogen interactions studies, RPMI 1640 Medium, no phenol red (ThermoFisher) with 2% of FBS was used. When desired, differentiated cells were stimulated for ROS production by using 10 μg/ml of phorbol 1-myristate 13-acetate (PMA, Sigma). When stated, 10 μg/mL cytochalisin D (Sigma) was used to inhibit phagocytosis. Permeabilization buffer containing PBS +0.2% saponin with or without 2% BSA was used for phagocytosis, NET, autophagic studies and bacterial survival evaluation.

Bacterial strains and cultures

The experiments were performed using these Gram-negative bacteria: *Moraxella catarrhalis* BBH18 (GenBank assembly accession: GCA_000092265.1) a seroresistant-lineage strain isolated from a sputum isolate from a COPD patient during an exacerbation (De Vries et al., 2010) and a clinical isolates and Nontypeable *Haemophilus influenzae* NTHi 658 coming from AERIS Study (Study ID: EPI-HIP 001 BOD UK) (Mayhew et al., 2018).*M. catarrhalis* was grown in Brain-Heart Infusion Broth (BHI) agar plates at 37°C with 5% CO2. BHI was used as fluid growth medium at 37°C, 185 rpm with 5% CO2. NTHi was grown on chocolate Haemophilus 2 agar (HAE2, BioMerieux) at 37°C with 5% CO2. Brain-heart infusion (BHI) broth (Difco Laboratories) supplemented with 10 μg/mL each of haemin (Sigma) and nicotinamide adenine dinucleotide (NAD, Sigma) was used as fluid growth medium. Bacteria concentration was determined by both measuring O.D. at 600 nm and colony forming units (CFU) by dilution plating. 0.5 $O.D._{600}$ has proved to be equivalent to 2 × 10^8 CFU /mL for BBH18 while 6 × 10^8 CFU/ml for NTHi 658. For all host-pathogen interactions studies, viable and exponentially-growing bacterial cells were used.

Ethical statement

The three human sera (ID:2543, 6002, 2151 from Phleb001_20180404-AXB-1805_Phleb001 generic) used in the study were obtained according to Good Clinical Practice in accordance with the declaration of Helsinki and patients have given their written consent for the use of the samples of study MENB REC 2ND GEN-074 (V72_92). The study was approved by the Western Institutional Review Board (WIRB). The sera have been pooled and used as human complement source for the research purpose. The studies involving venous blood from healthy human individuals (for neutrophils isolation) were reviewed and approved by a GSK commercial provider, CHU Tivoli (BELGIUM). The patients/participants provided their written informed consent to participate to further research. The age/developmental stage, sex, and gender identity of the subjects are not known.

Isolation of human neutrophils

Human neutrophils were isolated using a density gradient method. Blood was collected from healthy individuals, diluted 1:1 with Dulbecco's PBS (Sigma) and separated using a Ficoll gradient (Ficoll-plaque PLUS, 1.078 g/ml, GE Healthcare Life Science) and Histopaque 1,119 g/ml (Sigma). The layers containing plasma and peripheral blood mononuclear cells were aspirated carefully, preserving the erythrocyte/granulocyte layer. Hyperosmotic shock for erythrocytes lysis was performed with sterile cold water and PBS 10X. Finally, granulocytes were collected by centrifugation at 1,000 g for 5 min. The cell pellet was reconstituted in RPMI no phenol red (Gibco).

METHOD DETAILS

Phagocytosis studies by FACS

PMA-stimulated dHL-60 (1 × 10^6) were treated with 10 μg/mL cytochalisin D (Sigma) (for bacterial adhesion) or left untreated (total bacteria-dHL-60 interaction). They were infected with 5 × 10^7 CFU (MOI 50) of *M. catarrhalis* or NTHi bacterial cells for 20, 45 and 75 min in RPMI 1640 (no phenol red) + 2% FBS medium and incubated at 37°C in the presence of 5% CO_2. After incubation, samples were fixed with 4% (v/v) formaldehyde (Sigma) for 1 h and *M. catarrhalis* and NTHi bacteria were detected by staining for UspA2 or whole cell, respectively (rabbit polyclonal antibodies diluted 1:1000 in permeabilization buffer). Samples were incubated for 20–30min at RT in the dark with 100 μL of permeabilization buffer containing a secondary

rabbit anti-mouse immunoglobulin G (whole molecule) Alexa fluor 633-conjugated (Invitrogen) diluted 1:500. After two washes with PBS, dHL-60 were evaluated by flow cytometry and expressed as the percentage of Alexa Fluor 647 positive cells (untreated samples) or the percentage of cells with bacteria attached (cytochalisin D). The percentage of phagocytosis was calculated subtracting the percentage of adhesion to the total interaction. All data were collected using a BD FACS CANTO II (BD Bioscience) by acquiring 100,000 events, and the data analysed using the Flow-Jo software (v.8.6, TreeStar Inc).

Reactive oxigen species detection

Intracellular ROS with CellRox Deep red flow cytometric analysis and Extracellular ROS with a Luminol-dependent chemiluminescence (LDCL) assay

Differentiated HL-60 cells resuspended in phenol red free RPMI 1640 containing 2% FBS. Untreated and 10 μg/mL PMA-treated dHL-60 cells represented negative and positive controls for ROS production, respectively. Cells were also infected by *M. catarrhalis* or NTHi bacterial cells at different MOI.

For intracellular ROS, CellROX Deep Red Reagent (ThermoFisher) was added at a final concentration of 5 μM to differentiated cells (1×10^6/reaction) and incubate for 30 min at 37°C. dHL-60 cells were infected or not with *M. catarrhalis* or NTHi bacterial cells at MOI 50. At the time points indicated in the figure legends, samples were fixed with 4% (v/v) formaldehyde (Sigma) for 1 h and subsequently, the mean fluorescence intensity (MFI) at 633 nm was determined after having performed gates on viability (LIVE/DEAD Fixable Aqua Dead Cell Stain, 1:1000, ThermoFisher), morphology and non-aggregated cells. All data were collected using a BD FACS CANTO II (BD Bioscience) by acquiring 100,000 events, and the data analysed using the Flow-Jo software (v.8.6, TreeStar Inc).

For extracellular ROS, 2 mM luminol (Sigma) was used to monitor the kinetics of the oxidative stress response. Approximately 5×10^4 cells in 90 μL were seeded into a black flat 96-well microplate (costar) and infected or not with bacteria at a MOI 12, 25, 50 and 100. Luminescence was read in a TECAN Infinite 200 plate reader with settings of: 1,000-ms integration, reading every 3 min for 2h at 37°C.

To verify if bacteria-cells contacts or secreted bacterial products were required, dHL-60 cells were infected with *M. catarrhalis* at a MOI of 50 for 45 min in white RPMI or bacteria were simply grown to mid-exponential phase in BHI medium, respectively. The resulting supernatants were collected, passed through a 0.2 μm syringe filter and subsequently added to PMA-stimulated naïve cells. To examine whether bacterial internalization was needed, dHL-60 cells were pre-exposed to 10 μg/ml cytochalasin D (Sigma) for 15 min to inhibit phagocytosis. To verify if these human CEACAM1, Siglec-5 and Siglec-9 receptors are indeed those specifically bound by Mcat to dampen ROS production, we challenged PMA-activated dHL-60 cells (1×10^6 / reaction) with *M. catarrhalis* (MOI of 50), untreated or pre-incubated with 200 nM of each recombinant receptor. The intracellular ROS production was evaluated as previuosly described.

Flow cytometric analysis of *M. catarrhalis* engagement of human recombinant receptors CEACAM-1, Siglec-5 and Siglec-9

1×10^7 exponentially-growing *M. catarrhalis* bacterial cells were resuspended in PBS and incubated or not (naïve bacterial cells), overnight at 4°C, with 2 μg of each human recombinant protein (VWR): CEACAM-1 (as positive control), Siglec-5 and Siglec-9 inhibitory receptors. Samples were fixed with 4% (v/v) formaldehyde (Sigma) for 1 h and subsequently incubated for 1 h with rabbit antibodies specific to each recombinant receptor (rabbit anti-CEACAM1, anti-Siglec-5 and anti-Siglec-9; ThermoFisher) diluted 1:500 in PBS. Samples were incubated for 20–30min at RT in the dark with PBS containing a secondary goat anti-rabbit immunoglobulin G (whole molecule) Alexa fluor 488-conjugated (ThermoFisher) diluted 1:500. After two washes with PBS, binding of these soluble proteins to the bacteria was revealed by flow cytometry. All data were collected using a BD FACS CANTO II (BD Bioscience) by acquiring 100,000 events, and the data analysed using the Flow-Jo software (v.8.6, TreeStar Inc).

NET: quantification and visualization by confocal microscopy

dHL-60 cells (or primary cells) were resuspended in HBSS (ThermoFisher) medium and seeded in a 96-well plate. Untreated and 10 μg/mL PMA-treated cells represented negative and positive controls for NET production, respectively. Subsequently, untreated cells were infected with *M. catarrhalis* BBH18 or NTHi 658 individually at MOI 50 or in their combination (MOI 25 each). Cells were treated with PMA and infected or

not by *M. catarrhalis* (MOI50). The cells were incubated at 37°C in an incubator for 4 h (in the case of PMNs, 2 h). To quantify NET-structures, the supernatant was carefully removed, and the cells were treated with micrococcal nuclease (500mU/ml, ThermoFisher) for 15 min in the presence of $CaCl_2$ (1.5mM, Sigma). EDTA (5mM, Sigma) was added to inhibit nuclease activity. The amount of extracellular DNA in the supernatant of cells was then quantified using PicoGreen (ThermoFisher) staining; the fluorescence was detected using a TECAN Infinite 200 plate reader. Each sample was analysed in triplicate to avoid any bias in the reading. To visualize NET-structures, samples were spotted onto a POLYSINE slide (Menzel-Glaser). After 4 h, samples were fixed with 4% (v/v) formaldehyde (Sigma) for 1h then incubated for 1 h with the mouse monoclonal anti-myeloperoxidase (MPO) antibody diluted 1:1000 in PBS +5% BSA. Samples were washed with of PBS and incubated for 20–30 min at RT in the dark with 100 µL of PBS containing a secondary goat anti-mouse immunoglobulin G (whole molecule) Alexa fluor 488-conjugated (ThermoFisher) diluted 1:500. For the experiments performed with primary cells, adherent and not internalized *M. catarrhalis* and NTHi bacteria were detected by staining UspA2 or whole cell, respectively (rabbit polyclonal antibodies diluted 1:1000) with a secondary goat anti-rabbit immunoglobulin G (whole molecule) Alexa fluor 594-conjugated (ThermoFisher) diluted 1:500. After two washes with PBS, a droplet of a mounting solution containing DAPI was applied. The final step consisted in placing a cover glass on each spot and analysing the samples with a confocal ZEISS LSM700 microscope. 10 fields were observed, with at least 5 cells/field. Images of NET structures were analyzed using the ZEN software.

Autophagic response and intracellular survival assay

ROS-stimulated dHL-60 cells were non-infected or incubated with *M. catarrhalis* or NTHi individually at MOI 50 or in their combination (MOI 50 each) for 40 min after which 400 µg/ml gentamicin (Sigma) was added to inhibit growth of extracellular bacteria. After 20 min, medium was changed with new pre-warmed RPMI 1640 (no phenol red), supplemented with PMA. The reactions proceeded for 3 additional hours. Immediately after the removal of gentamicin (control groups) and after 3 h, samples were processed for autophagic response and bacterial intracellular survival. For the former, samples were fixed with 4% (v/v) formaldehyde (Sigma) for 1 h. then incubated for 1 h with the rabbit anti-LC3B antibody diluted 1:500 in permeabilization buffer. Samples were incubated for 20–30 min at RT in the dark with permeabilization buffer containing a secondary goat anti-rabbit immunoglobulin G (whole molecule) Alexa fluor 633-conjugated (Invitrogen) diluted 1:500. After two washes with PBS, LC3B expression levels were evaluated by flow cytometry. All data were collected using a BD FACS CANTO II (BD Bioscience) by acquiring 100,000 events, and the data analyzed using the Flow-Jo software (v.8.6, TreeStar Inc). For bacterial intracellular survival, dHL-60 cells were permeabilized and colony formation unit (CFU)/ml was determined by dilution plating on BHI and HAE2 agar for *M. catarrhalis* and NTHi, respectively.

Electron microscopy (EM)

The cells were fixed in 4% paraformaldehyde solution in PBS pH 7.2 overnight at 4°C, washed in PBS, post-fixed in 1% OsO_4 in water for 1 h at 4°C, dehydrated in an ascending alcohol series. For scanning electron microscopy (SEM) observations, samples were processed by critical point drying in a Balzer's CPD030. Samples were gold-evaporated in a Balzer's MED 010 sputterer and observed in a SEM Quanta 400 scanning electron microscope operating at 20 kV. For transmission electron microscopy (TEM) observations, after the alcohol series, samples were infiltrated and embedded in epon resin that was polymerized at 60 °C for 48 h. Ultrathin sections were cut from samples on a Reichert-Jung Ultracut E ultramicrotome. They were mounted on 200-mesh copper grids, routinely counterstained, and observed in a FEI Tecnai G2 SPIRIT transmission electron microscope at an electron accelerating voltage of 120 kV equipped with a Tvips TemCam F216.

Mcat and NTHi opsonization with human sera

$5*10^7$ of exponentially growing Mcat and NTHi bacteria were resuspended in DPBS +1%BSA +0.1% glucosio+0.5%Tween 20 with or without 10% of human sera, hereafter called NHS. Tre sera (ID: 2543, 6002, 2151) from Phleb001_20180404-AXB-1805_Phleb001 generic were pooled and used as complement source at 10%. After an incubation of 30 min at 37°C, bacteria were washed and then stained for 30 min using 1:200 of both Fluorescein isothiocynate (FITC) conjugated polyclonal anti-human C3 antibody and AlexaFluor 594 conjugated anti-human IgG, then washed and fixed with 2% paraformaldehyde. Labeled bacteria were analyzed by flow cytometry for the binding to C3b and human IgG antibodies using a BD FACSCantoII and results reported as mean fluorescence intensity (MFI). 2 h post-inefection, opsonized

and unopsonized bacteria were used to evaluate their uptake and intracellular ROS production in dHL-60 cells, in as described above.

QUANTIFICATION AND STATISTICAL ANALYSIS

All data are expressed as the mean and standard error of the mean. A one-way analysis of variance (ANOVA) was performed when multiple independent groups needed to be tested for their difference in the mean, student's t-tests were used for paired values (R version 3.6.0).$p < 0.05$ was considered to be significant.